

Figure 10.20 The deep-water surface-wave analog (d,f) of two shelf problems involving topographic Rossby waves in uniformly stratified rotating fluid: (a) stratified problem; (b) result of affine transformation; (c) result of rotation; (d) equivalent deep-water problem (velocity potential  $\phi$ ); (e) stratified problem; (f) equivalent deep-water problem (atmospheric pressure  $P_1$  must be maintained lower than  $P_2$  for physical realizability).

tion. This is the stratified analog of Eckart's (1951) nonrotating LSW study of waves over a sloping beach (section 10.4.6).

For beach slopes much smaller than the slope  $(\sigma/N)$  of (low-frequency) internal wave characteristics (10.43), Wunsch thus found that internal waves are refracted just like surface gravity waves by the shoaling relief and that refractively trapped edge modes occur. From the dispersion relation

$$\left(\frac{n\pi}{D_0}\right)^2 = \frac{N^2 - \sigma^2}{\sigma^2} (l^2 + k^2)$$

for plane internal waves of the form

$$w = \sin\left(\frac{n\pi z}{D_0}\right) \exp(-i\sigma t + ilx +iky)$$

over a uniform bottom  $D_0$ ,  $l$  must ultimately become imaginary if  $D_0$  is allowed to grow parametrically offshore while  $n$  and  $k$  are held fixed. One would therefore expect a WKB treatment of internal waves over gently shoaling relief to result in refraction and refractive trapping *provided* that the mode number  $n$  does not

change, i.e., provided that the relief does not scatter energy from one mode into others. Constancy of  $n$  is indeed a feature of Wunsch's solutions but it cannot be expected to hold for more abrupt relief, especially if the relief slope exceeds the characteristic slope. If the relief couples modes efficiently, then scattering into higher modes allows  $l$  to remain real even in deep water far from shore so that energy is not refractively trapped near the coast. In principle, scattering into internal modes thus even destroys the perfect trapping of long surface gravity waves predicted by LSW theory over a step shelf, but in practice appreciable trapping is often observed. The efficiency of mode coupling depends both on the relief and on the vertical profile  $N(z)$  of the buoyancy frequency, so that a general result for internal waves is difficult to formulate.

### 10.4.8 Free Oscillations of Ocean Basins

Finding the free oscillations allowed by LTE in rotating ocean basins is difficult even in the  $f$ -plane (section 10.4.2). Platzman (1975, 1978) has developed powerful numerical techniques for finding the natural frequencies and associated flow fields of free oscillations allowed by LTE in basins of realistic shape and bottom relief. The general classification of free oscillations into first- and second-class modes characteristic of the idealized cases discussed in sections 10.4.2 and 10.4.5 (effectively for a global basin) persists in Platzman's (1975) calculations. For a basin composed of Atlantic and Indian Oceans, there are 14 free oscillations with periods between 10 and 25 hours. Some of these are very close to the diurnal and semidiurnal tidal periods, and all of them, being within a few percentage points of equipartition of kinetic and potential energies, are first-class modes. There are also free oscillations of much longer period, for which potential energy is only about 10% or even less of kinetic energy; they are second-class modes.

I know of no extratidal peaks in open-ocean sea-level records that correspond to these free oscillations. There is some evidence in tidal admittances for the excitation of free modes but the resonances are evidently not very sharp (see section 10.5.1). Munk, Bryan, and Zetler (private communication) have searched without success for the intertidal coherence of sea level across the Atlantic that the broad spatial scale of these modes implies. The modes are evidently very highly damped.

## 10.5 The Ocean Surface Tide

### 10.5.1 Why Ocean Tides Are of Scientific Interest

The physical motivation for studying and augmenting the global ensemble of ocean-tide records has expanded enormously since Laplace's time. In this section I have tried to sketch the motivating ideas without getting

involved in the details of theoretical models; some of these receive attention in subsequent sections.

Certain of the ancients knew a great deal about tides [see, e.g., Darwin's (1911a) summary of classical references], but the first extant reduction of observations made explicitly for predictive purposes may be the table of "flod at london brigge" due to Wallingford who died as Abbot of St. Alban's in 1213 (Sager, 1955). Making practical tide predictions was probably *the* preoccupation of observers for the next 500 years.

In 1683, Flamsteed (Sager, 1955) produced a table of high waters for London Bridge as well as, in the following year, corrections making it applicable to other English ports. Darwin (1911a) quotes Whewell's description, written in 1837, of how successors to Flamsteed's tables were produced:

The course . . . would have been to ascertain by an analysis of long series of observations, the effects of changes in the time of transit, parallax, and the declination of the moon and thus to obtain the laws of phenomena.

. . . Though this was not the course followed by mathematical theorists, it was really pursued by those who practically calculated tide tables. . . . Liverpool London, and other places had their tables, constructed by undivulged methods . . . handed down from father to son.

. . . The Liverpool tide tables . . . were deduced by a clergyman named Holden, from observations made at that port . . . for above twenty years, day and night. Holden's tables, founded on four years of these observations, were remarkably accurate.

At length men of science began to perceive that such calculations were part of their business. . . . Mr. Lubbock . . . , finding that regular tide observations had been made at the London docks from 1795, . . . took nineteen years of these . . . and caused them to be analyzed. . . . In a very few years the tables thus produced by an open and scientific process were more exact than those which resulted from any of the secrets.

Quite aside from its proprietary aspects, Darwin (1911b) explicitly notes the synthetic nature of this process; it at least conceptually represents "the oscillation of the sea by a single mathematical expression" provided by Bernoulli in 1738 for an inertialess ocean (the equilibrium tide), by Laplace for a global ocean obeying Newton's laws of motion, and assumed to exist for actual oceans even if too complex to represent in simple form.

Kelvin, in about 1870 (Darwin, 1911b) introduced the harmonic method, which Darwin (1911b) calls "analytic" because synthesis of the entire tide into one dynamically derived form is abandoned and instead the tide at any given place is regarded as a sum of harmonic oscillations whose frequencies are determined from astronomy (section 10.2) but whose amplitudes and phases must be determined from analysis of *in situ* sea-

level observations. Prediction is then carried out by recombining the harmonic oscillations at future times.

Kelvin's suggested procedure was made feasible by the introduction of recording tide gauges in which the motion of a float in a well, insulated from short-period waves but otherwise freely connected with the sea, drives a pencil up and down a paper wrapped on a drum rotated by clockwork, thus producing a continuous plot of sea level versus time. [Darwin (1911a) describes contemporary instruments.] Harmonic analysis of this record at *relatively few astronomically determined frequencies* was feasible by judicious sampling and manual calculation. The recombination of harmonics at future times was then carried out mechanically by means of a series of pulleys, movable at frequencies corresponding to the astronomical ones, that drove a pencil over a paper wrapped on a drum rotated by clockwork, thus ultimately providing a plot of predicted sea level versus time. The design of such a machine was due to Kelvin, and elaborations were in regular use until the mid-1960s (Zetler, 1978).

Even before Kelvin's introduction of the harmonic method, Lubbock and Whewell (Darwin, 1911b) had begun to combine observations at different ports into cotidal maps showing the geographical variation of sea level associated with tides. Thus Airy in 1845 gave a chart (modified by Berghaus in 1891) of locations of high water at different times of day in the North Sea (figure 10.21). Concerning this, Darwin (1911b) remarks, "It will be noticed that between Yarmouth and Holland the cotidal lines cross one another. Such an intersection of lines is in general impossible; it is indeed only possible if there is a region in which the water neither rises nor falls. . . . A set of observations by Captain Hewitt, R.N. made in 1840 appears to prove the existence of a region of this kind." This is probably the first recorded observation of an amphidromic point.

But hourly maps of high-water locations change throughout the month. Kelvin's harmonic analysis decomposed the tide into harmonic components for which a single cotidal map, with cotidal lines drawn at fractions of the period of the component, can represent the entire spatial variation of that component forever. Time series at thousands of ports may thus be reduced to a handful of global maps that are ideal summaries of observations for comparison with solutions of LTE forced by the different harmonic components of the ATGF. Kelvin's abandonment of the "synthetic" viewpoint thus in effect provided the means for its reinstatement.

Of the handful of such maps constructed empirically for global tides, Dietrich's (1944) are perhaps the most widely quoted. Villain (1952) gives an extensive discussion of the observations leading to his global  $M_2$  cotidal map (figure 10.22). Much modern tidal research has consisted of attempts to apply the principles of

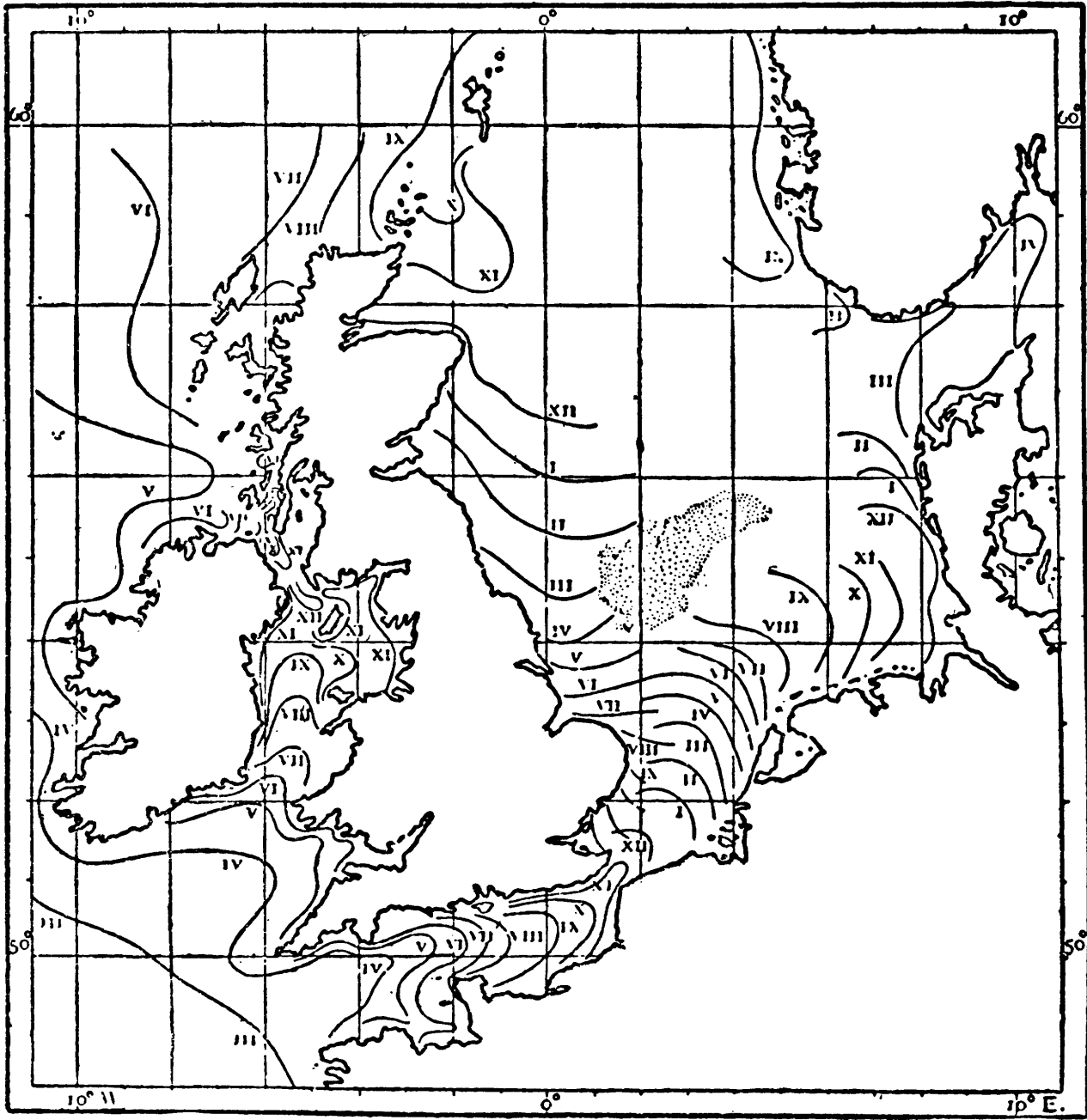


Figure 10.21 Airy's chart of cotidal lines in British seas. (Darwin, 1911b.)

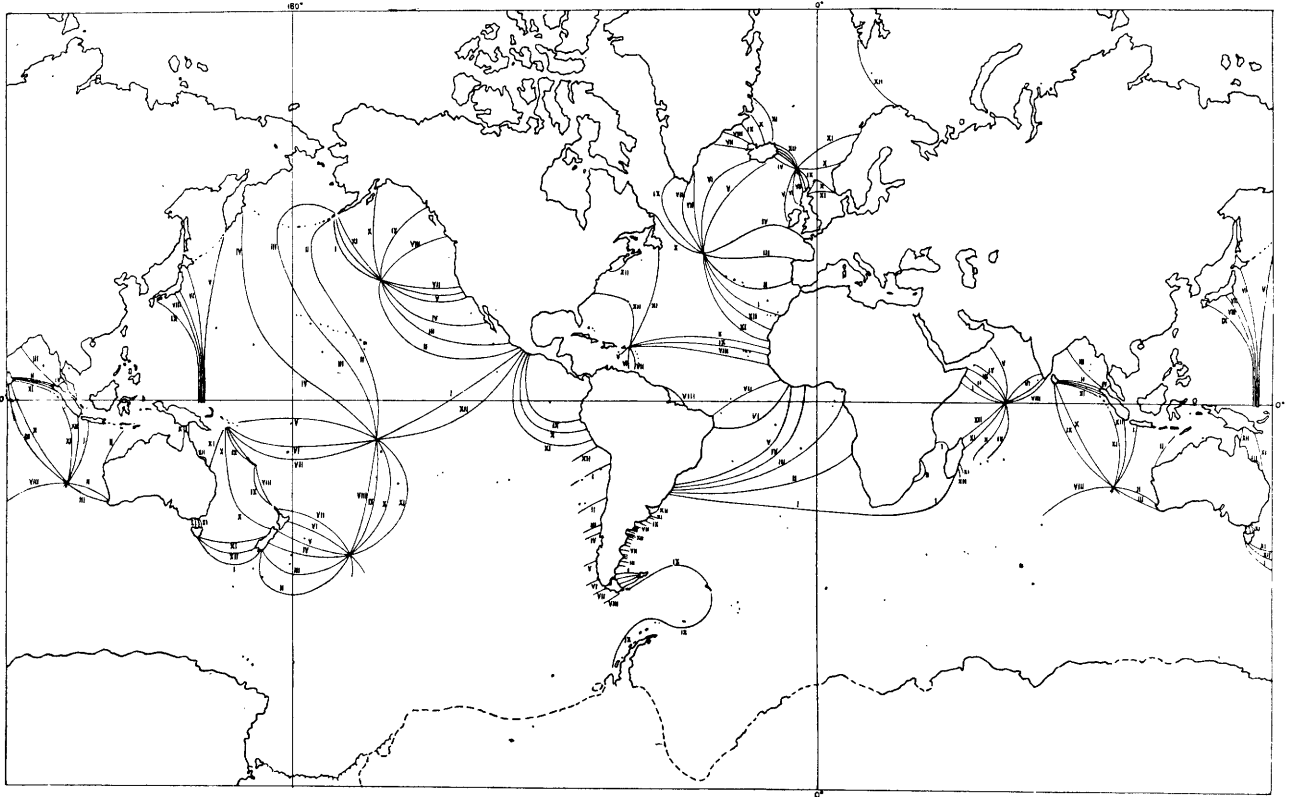


Figure 10.22 Cotidal lines for  $M_2$  (in lunar hours relative to moon's transit over Greenwich). (Villain, 1952.)

dynamics to reproduce and hence to “explain” the global distribution of tides as suggested by such empirical maps. But the degree of success achieved to date, as well as insight into the variation of the dynamics of tides over the globe, has required thinking about how the response of the ocean would change if tidal frequencies could be varied. Since they cannot be, this implies comparing global tidal maps at different tidal periods. The origins of this viewpoint are found in the work of Munk and Cartwright (1966), who were enabled by the advent of modern computers to analyze 19 years of hourly tide readings at Honolulu and Newlyn “without astronomical prejudice as to what frequencies are present and what are not, thus allowing for background noise.”

Their work has been influential in two very general ways quite apart from the improvement in tide prediction that it introduced. First, it provided a clear distinction between sea-level fluctuations due to TGF and those of similar period due to nontidal agents, a distinction crucial in establishing the significance of any geophysical interpretation of all but the strongest constituents of ocean or solid-earth tides. Second, it introduced the idea of oceanic admittance, the (possibly complex) ratio between ocean response and forcing, as a continuous function of frequency that can be estimated from tidal observations and that summarizes

the dynamic response of the ocean to time-variable forcing in a manner easily related to the properties of free solutions of LTE by an expansion in eigenfunctions.

If the ocean had many sharp resonances within the frequency bands spanning the three species, the tidal admittance would have amplitude peaks and rapid phase shifts. Typical deep-sea admittances tend to be smooth across a species but are far from constant. Admittance curves for the Coral Sea (Webb, 1974) and at Bermuda (Wunsch, 1972c) are shown in figures 10.23A and 10.23B, respectively. The Coral Sea admittance is unusual in its very sharp sudden variation between  $M_2$  and  $S_2$ , apparently showing the existence of a sharp local resonance. The amplitude of the Bermuda admittance rises smoothly, by 400% toward lower frequencies over the semidiurnal band; Wunsch's result is consistent with Platzman's (1975) prediction of an Atlantic resonance of roughly 14-hour period, but one appreciably broadened by dissipation.

Smoothness of the admittance across tidal bands was anticipated by Munk and Cartwright (1966) in their “credo of smoothness”: “We do not believe, nor will we tolerate, the existence of very sharp resonance peaks.” In part, this credo had its origin in the prevailing beliefs, since then largely confirmed, that ocean

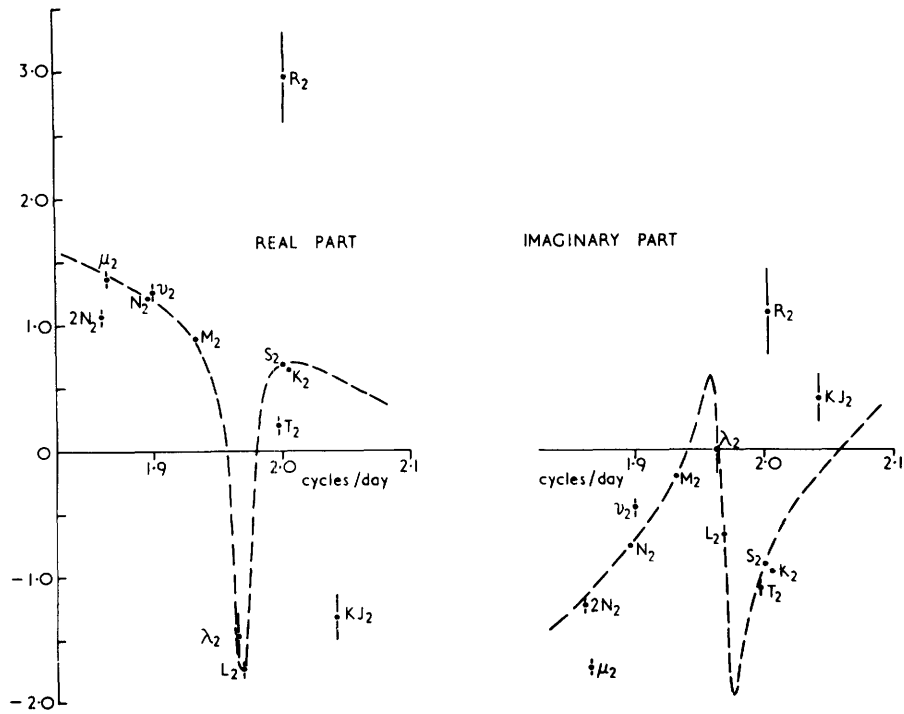


Figure 10.23A The real and imaginary parts of the response function at Cairns (16°55'S, 145°47'E), showing a resonance in the Coral Sea. (Webb, 1974.)

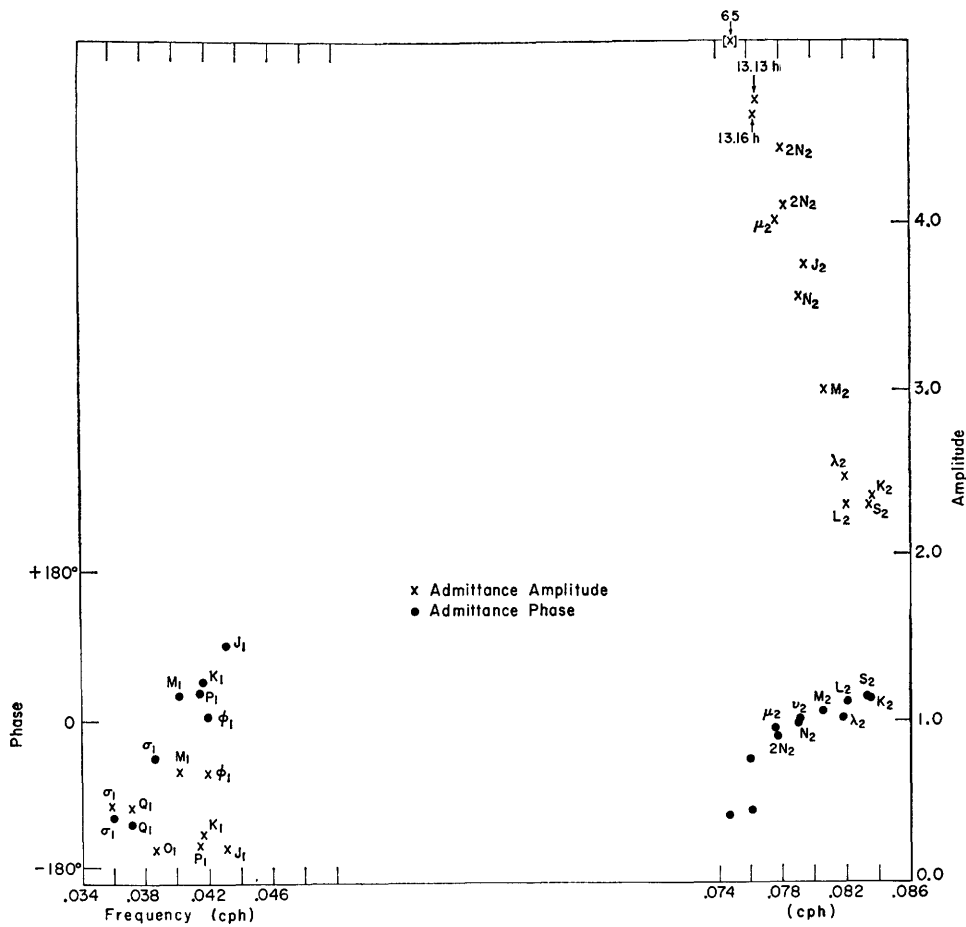


Figure 10.23B Amplitude and phase of the admittance at Bermuda. (Wunsch, 1972c.)

tides must be of rather low  $Q$ . Evaluation of  $Q$  requires knowledge of the total energy  $E$  stored in the tide as well as the rate  $\dot{E}$  at which it is dissipated; then

$$Q = \frac{2\pi E}{\dot{E}T}.$$

Estimation of the stored energy  $E$  was difficult before modern numerical solutions of LTE because of the open-ocean detail required. Earliest estimates assumed the tide to be in equilibrium; allowance for (likely) equipartition between potential and kinetic energy and for the area of the oceans led to an estimate of  $5.6 \times 10^{16}$  J for  $M_2$  (Garrett and Munk, 1971). I interpolated coastal  $M_2$  harmonic constants over the globe by solving LTE with these as boundary values and thus obtained (Hendershott, 1972) an estimate of  $7.29 \times 10^{17}$  J. But my kinetic energy was over twice my potential energy and I now believe this to have been a numerical artifact, especially since Platzman's (1975) near-tidal normal modes are within a few percentage points of equipartition. My estimate should thus be revised to  $5.14 \times 10^{17}$  J. Parke and Hendershott (1980) improved the interpolation by taking island data into account and found  $2.68 \times 10^{17}$  J (assuming equipartition).

The estimation of  $\dot{E}$  historically has been of importance in cosmology. Halley in 1695 first discovered that the apparent position of the moon is *not* that predicted by (frictionless) Newtonian mechanics. The discrepancy is real; Munk (1968) outlines ultimately unsuccessful attempts to resolve it by appealing to perturbation of the moon's orbit by changes in the earth's orbit around the sun. Much of the discrepancy is now believed to be due to tidal friction. As Immanuel Kant noted in 1754, tidal friction must slow the earth's daily rate of rotation; this alone gives rise to an apparent perturbation of the moon's mean longitude. By the conservation of angular momentum, the moon's angular velocity about the earth-moon center of mass is also altered and (for the present prograde rotation of the moon about the earth) the moon recedes from the earth (by about  $6 \text{ cm yr}^{-1}$ ; Cartwright, 1977). Müller (1976) reviews astronomical data both ancient (eclipse observations) and modern, and analyzes them simultaneously to estimate  $\dot{n}_t$  (the tidal acceleration of the moon's longitude  $n$ ),  $\dot{\Omega}/\Omega$  (the observed apparent acceleration of the earth's rotation frequency  $\Omega$ ),  $\dot{\Omega}/\Omega_{\text{TNT}}$  (the nontidal part of  $\dot{\Omega}/\Omega$ ), and  $\dot{G}/G$  (the possible rate of change of the gravitational constant  $G$ ). He finds

$$\dot{n}_t = -27.2 \pm 1.7'' \text{ cy}^{-2},$$

$$\dot{\Omega}/\Omega = -22.6 \pm 1.1 \times 10^{-11} \text{ yr}^{-1},$$

the latter corresponding to a lengthening of day of  $2.0 \times 10^{-3} \text{ s cy}^{-1}$ . If he assumes  $\dot{G}/G = 0$ , then  $\dot{\Omega}/\Omega_{\text{TNT}}$  becomes  $9.2 \pm 2.5 \times 10^{-11} \text{ yr}^{-1}$ , a sizable portion of  $\dot{\Omega}/\Omega$  that demands geophysical explanation. Various cos-

mological theories have  $\dot{G}/G$  of order  $5 \times 10^{-11} \text{ yr}^{-1}$ ;  $\dot{\Omega}/\Omega_{\text{TNT}}$  then becomes zero with an uncertainty of order  $5 \times 10^{-11} \text{ yr}^{-1}$ . "It appears that either we really have a (non zero) cosmological constant  $\dot{G}/G$  consistent with the Hubble constant, or we have a significant  $\dot{\Omega}/\Omega_{\text{TNT}}$ " [Müller (1976)].

Lambeck (1975) gives expressions for the tidally induced rates of change of the semimajor axis  $a$  of the moon's orbit, of its eccentricity  $e$ , and of its orbital inclination  $i$  in terms of a spherical harmonic decomposition of the ocean tide  $\zeta_0$ . For semidiurnal tides only the second harmonic is important. Once these rates of change have been estimated, then  $\dot{n}_t$  and  $(\dot{\Omega}/\Omega)_t$  (i.e., the tidal part of  $\dot{\Omega}/\Omega$ ) may be estimated from, respectively, Kepler's law (Cartwright, 1977, equation 8.3) and from the conservation of angular momentum (Lambeck, 1977, equations 2).  $\dot{n}_t$  and  $(\dot{\Omega}/\Omega)_t$  imply a rate  $\dot{E}_t$  of tidal energy dissipation in the earth-moon system (Lambeck, 1977, equations 3). Using global calculations of  $\zeta_0$  for the  $M_2$  ocean tide by Bogdanov and Magarik (1967), by Pekeris and Accad (1969) and by myself (Hendershott, 1972), Lambeck (1977) thus estimates for  $M_2$

$$\dot{n}_t = -27.8 \pm 3'' \text{ cy}^{-2} \quad (\text{his table 7}),$$

$$(\dot{\Omega}/\Omega)_t = -25.8 \times 10^{-11} \text{ yr}^{-1} \quad (\text{his table 8}),$$

$$\dot{E}_t = 3.35 \times 10^{19} \text{ erg s}^{-1} \quad (\text{his equation 3b}).$$

Since his work, new  $M_2$  calculations by Accad and Pekeris (1978) and by Parke and Hendershott (1980) have appeared. These calculations include ocean self-attraction and loading (section 10.5.3) and are not unrealistically resonant. Accad and Pekeris (1978) directly evaluate the flow of  $M_2$  energy out of the numerical ocean and obtain  $2.44\text{--}2.79 \times 10^{19} \text{ erg s}^{-1}$ . Parke and Hendershott (1980) evaluate the rate  $\langle \dot{W} \rangle$  at which the  $M_2$  tide generating forces (potential  $\Gamma$ ) and ocean floor (solid earth  $M_2$  tide  $\delta$ ) do work on the ocean averaged  $\langle \langle \rangle \rangle$  over a tidal period

$$\langle \dot{W} \rangle = \iint_{\text{ocean}} \left( \rho \left\langle \Gamma \frac{\partial \zeta_0}{\partial t} \right\rangle + \rho g \left\langle \zeta_0 \frac{\partial \delta}{\partial t} \right\rangle \right) dA$$

(Hendershott, 1972) and obtain  $2.22 \times 10^{19} \text{ erg s}^{-1}$ . All this work is lost in tidal friction. If these results are taken as an improved estimate  $\dot{E}'_t$  of  $\dot{E}_t$  for the  $M_2$  tide

$$\dot{E}'_t = 2.2\text{--}2.8 \times 10^{19} \text{ erg s}^{-1},$$

then Lambeck's (1975) procedure would yield

$$\dot{n}'_t = -(18.3\text{--}23.2)'' \text{ cy}^{-2},$$

$$(\dot{\Omega}/\Omega)'_t = -(16.9\text{--}21.6) \times 10^{-11} \text{ yr}^{-1}$$

for  $M_2$ . If we retain unaltered Lambeck's (1977) estimate of the contribution  $\Delta \dot{n}$  and  $\Delta(\dot{\Omega}/\Omega)_t$  of all remaining tides to  $\dot{n}_t$  and  $(\dot{\Omega}/\Omega)_t$ ,

$$\Delta \dot{n} = -3.1'' \text{ cy}^{-2},$$

$$\Delta(\dot{\Omega}/\Omega) = -6.9 \times 10^{-11} \text{ yr}^{-1},$$

then we obtain the revised estimates for all tides:

$$n_t = [21.4-26.3]'' \text{ cy}^{-2},$$

$$(\dot{\Omega}/\Omega) = -(23.8-28.5) \times 10^{-11} \text{ yr}^{-1}.$$

These are to be compared with Müller's (1976) estimates from astronomical data:

$$\dot{n}_t = -27.2'' \text{ cy}^{-2}$$

and

$$(\dot{\Omega}/\Omega)_t = -(13.4-22.6) \times 10^{-11} \text{ yr}^{-1}$$

for

$$\dot{G}/G = -(0-6.9) \times 10^{-11} \text{ yr}^{-1}.$$

The comparison is worst if  $\dot{G}/G$  is taken zero and becomes rather good if  $\dot{G}/G$  is allowed to differ from zero.

There is thus some interest in estimating  $\dot{E}$  for ocean tides but, as indicated above, results differ significantly depending on details of the estimation procedure. The estimates referred to above (except for that of Accad and Pekeris, 1978) essentially use global cotidal maps to find the part of the ocean tide in phase with the tide generating forces. The resulting rate of working  $\dot{W}$  is then attributed to friction without having to localize it anywhere. Indeed, the long waves making up the tide transmit energy over the globe so readily that we may expect no correlation between where the moon and sun work hardest on the sea and where the energy thus put into the sea is dissipated.

It may be that little of that dissipation occurs in the open ocean. Taylor (1920) estimated tidal friction in the Irish Sea and showed that most of the energy thus lost comes from the adjacent deep ocean with little direct input due to local working by moon and sun. His methods were extended to the world's coasts and marginal seas by Jeffreys (1921), Heiskanen (1921), and Miller (1966). Miller finds  $\dot{E} = 0.7-2.5 \times 10^{19} \text{ erg s}^{-1}$ , two-thirds of which occurs in the Bering Sea, the Sea of Okhotsk, the seas north of Australia, the seas surrounding the British Isles, the Patagonian shelf, and Hudson Bay. This is below all but the most recent estimates of  $\langle \dot{W} \rangle$ . It should be, by perhaps 10%, because of open-ocean internal tidal dissipation not consistently or completely taken into account (section 10.6). It is now difficult to say whether or not the difference indicates an important omission of some dissipative mechanism.

Additional information about tidal dissipation is contained in the width of conjectured or observed peaks in the admittance amplitude and in shifts in phase of the admittance from one constituent to another. Thus the width of the amplitude-response curve

at Bermuda (figure 10.23B; Wunsch, 1972c) suggests a local  $Q$  exceeding about 5. Garrett and Munk (1971) surveyed the difference in admittance phase between  $M_2$  and  $S_2$  (the age of the tide) and concluded that worldwide semidiurnal tides had a  $Q$  of order 25. Webb (1974) argued that such age-derived estimates of  $Q$  primarily reflect localized resonances. It is thus difficult to compare such results with the global  $Q$ , for  $M_2$ , with a  $Q$  of 17 emerging from the most recent cotidal chart of Parke and Hendershott (1980).

Astronomical and oceanographic interest in the amount and geographical distribution of tidal friction constitutes one of the principle modern motivations for studying ocean tides. The other principle motivation is the need, by solid-earth tidalists (Farrell, 1979) and satellite geodesists (Marsh, Martin, McCarthy, and Chovitz, 1980) for a very accurate map of the global distribution of ocean tides. Significant improvement of the most recent numerical maps is going to require extensive new observations.

The technology of deep-ocean pressure sensors suitable for gathering pelagic tide records was pioneered by Eyriés (1968), F. E. Snodgrass (1968) and Filloux (1969). The latest compilation of such results (Cartwright, Zetler, and Hamon, 1979) summarizes harmonic constants for 108 sites irregularly distributed around the world. Cartwright (1977) reviews the history and considerable accomplishments of pelagic tide recording but concludes that economic and political difficulties as well as rapidly evolving research priorities make it an unlikely method for detailed global tide mapping.

Several alternative methods are beginning to be studied. Given a sufficient number of measurements of the solid-earth tide, it is possible to construct estimates of the ocean tide that (in part) generated the solid-earth tide. But high precision earth-tide measurements are needed, and ocean tides in the vicinity of coastal earth-tide stations must be accurately known in order to perceive global ocean tide contributions (Farrell, 1979). Kuo and Jachens (1977) document attempts along these lines.

Satellites may be employed to study ocean tides in two ways. First, the periodic tidal deformation of earth and ocean results in significant perturbation in the orbits of close satellites (Cazenave, Daillet, and Lambeck, 1977). The lowest-order spherical-harmonic components of the tide are the most accessible by this method. It therefore complements the second possibility, direct measurement of satellite-to-sea-surface altitude. The greatest obstacle to extraction of ocean tides from such altimetry is not the error in the altitude measurement but rather the error in our knowledge of where the satellite is relative to the center of the earth. This "tracking" or "orbit" error is greatest at a spatial

scale corresponding to the earth's circumference but decreases rapidly at smaller spatial scales. It probably makes the large-scale features of ocean tides inaccessible from the GEOS-3 altimetry-data set. But smaller-scale tidal systems appear to be directly observable from the later SEASAT-1 altimetry. Parke has permitted me to reproduce (figure 10.24) his recovery of tides along the Patagonian shelf from SEASAT-1 altimetry (Parke, 1980) as an example.

Determining the combination of ocean-tide gauge data (coastal, island, and pelagic), of earth-tide data, of satellite-orbit perturbations, and of satellite altimetry optimal for mapping ocean tides and localizing their dissipation is now perhaps the outstanding theoretical problem in ocean tides.

### 10.5.2 Partial Models of Ocean Tides

**Introduction** In his George Darwin lecture "The Tides of the Atlantic Ocean," Proudman (1944) stated, "I shall mainly be concerned with the discovery of the distribution of tides over the open Atlantic Ocean, by the application of the principles of dynamics."

This was, of course, Laplace's goal for global tides. From Laplace's time until now, many researchers have pursued this goal with dogged persistence by solving LTE with astronomical forcing for oceans having shape and relief sufficiently idealized that existing methods of solution could produce an evaluable answer. With hindsight, the properties of these solutions may be appreciated by regarding the solution as eigenfunction expansions in which the various eigenfunctions  $Z_n(\phi, \theta) \exp[-i\sigma_n t]$  or free oscillations allowed by LTE have the properties summarized in section 10.4. The frequency  $\sigma_n$  of oscillation is the most natural eigenparameter, but the eigenfunction expansion  $\zeta(\phi, \theta, t) = \sum_n a_n Z_n \exp[-i\sigma_n t]$  for a tide forced at frequency  $\sigma_T$  is *not* of the usual form in which (in the absence of dissipation)  $a_n \sim (\sigma_T^2 - \sigma_n^2)^{-1}$ . If however, for a given frequency  $\sigma_T$  of forcing, the inverse  $\Delta^{-1}$  of the mean depth

$$\Delta \equiv (4\pi)^{-1} \iint D(\phi, \theta) \cos \theta d\theta d\phi$$

$[D(\phi, \theta) = 0 \text{ on land}]$  is regarded as the eigenparameter with "resonant" depths  $\Delta_n$ , then  $a_n \sim (\Delta^{-1} - \Delta_n^{-1})^{-1}$ . Nothing restricts  $\Delta_n$  to positive values. Indeed, negative-depth modes having  $\Delta_n < 0$  often exist and may be important in the eigenfunction expansion of forced solutions. This evidently was pointed out first by Lindzen (1967) for atmospheric tides.

Direct numerical solution of LTE in realistically shaped basins may be viewed as summation of this eigenfunction expansion, and has gone some distance toward attaining Proudman's stated goal. But Proudman's George Darwin lecture marked an important break with the sequence of dynamic studies that have since culminated in modern numerical solutions.

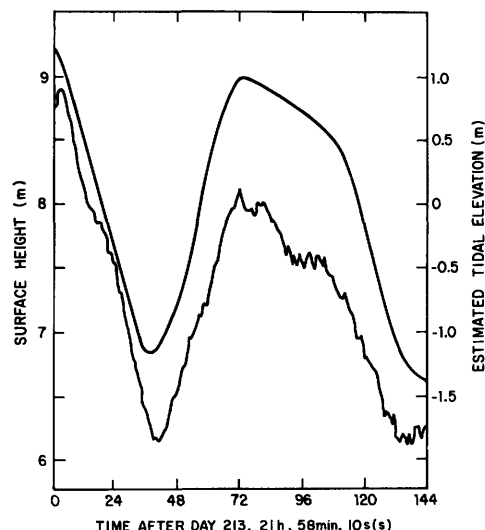
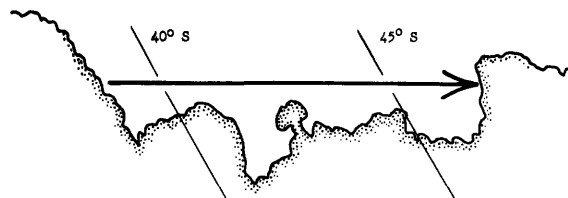


Figure 10.24 SEASAT altimeter record (wiggly line) and a reconstruction (smooth lines) from coastal harmonic constants of nearshore Patagonian shelf tides at the subsatellite point for the SEASAT pass whose path is shown in the upper panel. (Parke, 1980.)

Rather than solving LTE for Atlantic tides, Proudman computed free and forced  $M_2$  solutions of LTE for a portion of the Atlantic and fitted their sum to observations. Subsequent studies carried out in the same spirit but for more simple continental-shelf and marginal-sea geometries have provided dynamically understandable rationalizations for the distribution of tides in these regions and have led to a reappraisal of both observations and of global solutions of LTE. Discussion of these matters occupies the remainder of this section.

**Tides in the Gulf of California** Godin (1965) and Hendershott and Speranza (1971) noted that (10.29) is satisfied for all the Poincaré channel modes  $n = 1, 2, \dots$  in many of the world's long and narrow marginal seas. In these, then, all Poincaré modes are evanescent so that the tide away from the ends of the basin must be mainly a sum of two oppositely traveling Kelvin waves, usually of unequal amplitude. Friction in the basin (or a net rate of working on the tide-generating body by tides in the basin) will make the outgoing Kelvin wave of lower amplitude than the incoming one and will shift amphidromic points (at which the two Kelvin waves interfere destructively) toward the "outgoing" coast.

Figure 10.25 illustrates application of these ideas to the  $M_2$  tide in the Gulf of California. The westward displacement of the amphidromes points to substantial dissipation in the upper reaches of the Gulf. But this Kelvin wave fit does not well represent the tide there. On the basis of his extensive network of tide-gauge observations, Filloux (1973a) was able to estimate the tidal prism and mass transport for six sections along the length of the Gulf and could thus directly evaluate stored energy and energy flux along the Gulf, and energy flux from the moon into dissipation. About 10% of the energy entering the mouth from the Pacific ( $4.7 \times 10^{16}$  ergs $^{-1}$ ) is lost as the Gulf  $M_2$  tide works on the moon; the remainder is dissipated frictionally (over 80% northward of the islands in figure 10.25).

Elementary considerations suggest that the Gulf of California has a resonance fairly close to the semidiurnal tidal frequency. Filloux (1973a) estimates a  $Q$  of about 13 for the thus nearly resonant  $M_2$  tide. Stock (1976) constructed a finite-difference model of Gulf tides using a very fine (10-km) mesh. His solutions effectively sum both of the Kelvin waves and all the evanescent Poincaré modes as well as allowing for their

distortion by the irregular shape of the basin. He included dissipative effects and specified the elevation across the mouth of the Gulf in accordance with observations. His model is resonant at about 1.8 cpd with a  $Q$  sufficiently high that different discretizations of the problem, all a priori equally reasonable, can give very different Gulf tides. He found it necessary to force his model to have a realistic resonant frequency—fixed by arbitrarily varying the mean depth—before it would produce realistic cotidal maps (figure 10.26). Once this had been done, he found small but nevertheless significant sensitivity of the solution to the localization of dissipation; the solution agreeing best with Filloux's data was that in which most of the dissipation took place around the islands in the upper portion of the Gulf.

**The Boundary-Value Problem for Marginal Sea Tides** The Gulf of California is one of many marginal seas that connect with the global ocean across a relatively small mouth. Dynamic models of tides in such regions have generally been constructed by solving LTE in the region subject to the condition that the elevation

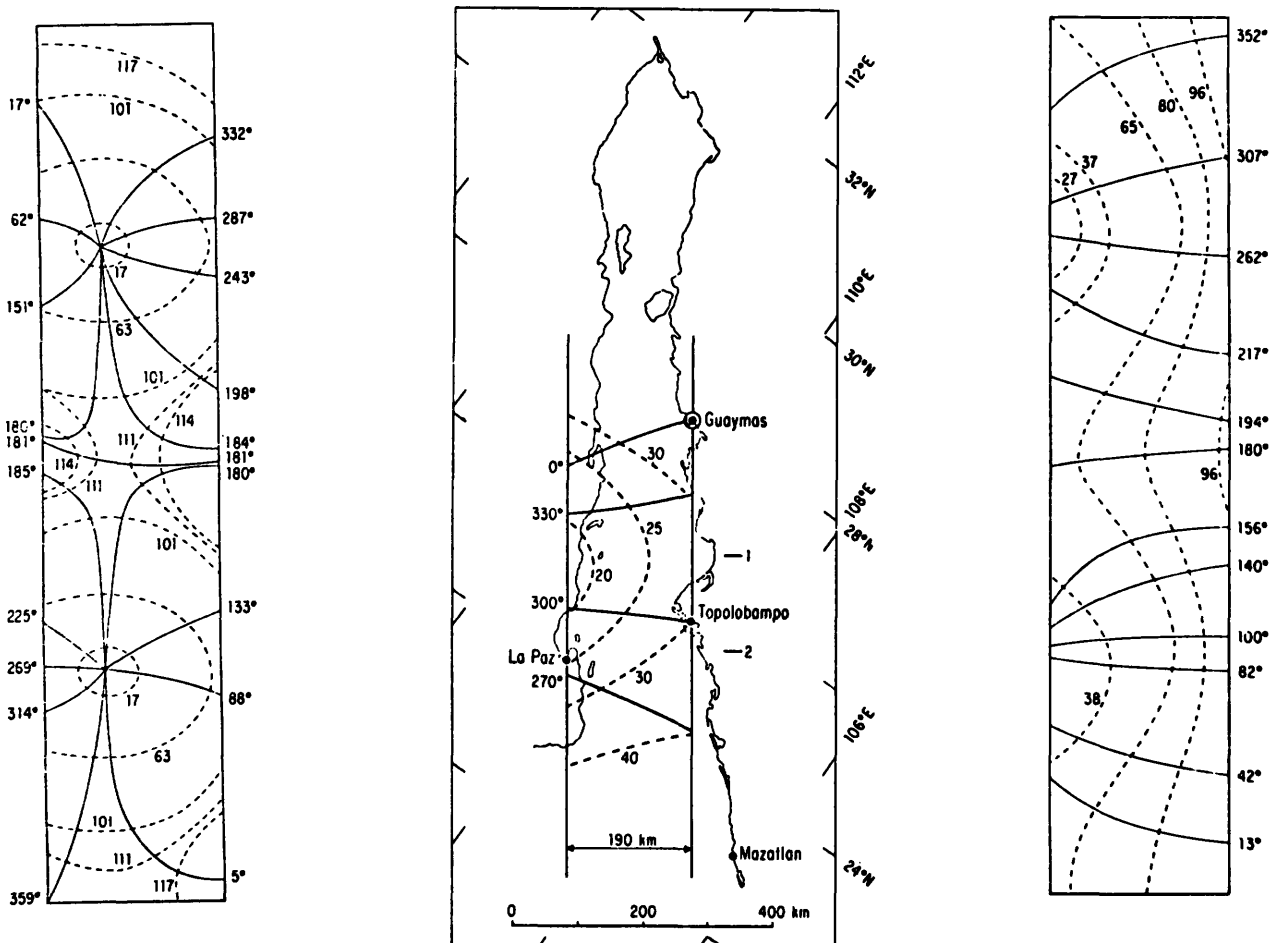


Figure 10.25 Left and right panels are co-oscillating tides in a rectangular gulf with little (left panel) and much (right panel)

absorption at upper boundary. Center panel is a Kelvin wave fit to  $M_2$  as observed in the Gulf of California.

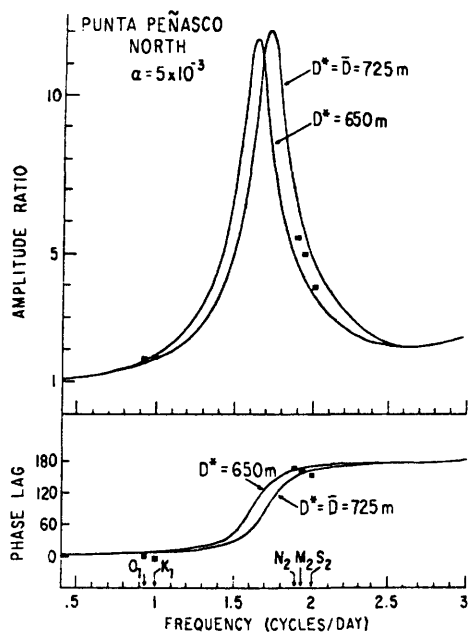


Figure 10.26 A comparison of the tidal response at Punta Peñasco (solid squares) with the tide at the mouth of the Gulf of California for two numerical models with different mean depths.

across the open mouth is equal to that actually observed. This is disadvantageous for two reasons. First of all, it eliminates damping of the marginal sea tide by radiation into the deep sea; second, it results in solutions that cannot predict the effects of changes in basin geometry (i.e., installation of causeways, etc.) on the tides because the tide across the open mouth is not allowed to respond to them.

Garrett (1974) pointed out that in many cases these difficulties may be resolved partially by allowing the marginal sea to radiate into an idealized deep sea. For a given constituent, suppose that, with forcing included and all other boundary conditions (i.e., no mass flux through coasts) satisfied, the mass flux  $\alpha\delta(S - S')$  normal to the mouth (across which distance is measured by  $S$ ) would result in the tide  $\zeta_G(S) + \alpha K_G(S, S')$  across the mouth when the marginal-sea problem is solved and would result in  $\zeta_D(S) + \alpha K_D(S, S')$  when the deep-sea problem is solved. The tides  $\zeta_G(S)$  and  $\zeta_D(S)$  are thus those that would result just inside and just outside across the mouth if it were closed by an imaginary impermeable barrier. In the real world, the mass flux  $U(S)$  across the mouth is fixed by the necessity that its incorporation into either the marginal-sea or the deep-sea problem give the same tide  $\zeta_M(S)$  across the mouth:

$$\begin{aligned} \zeta_M(S) &= \zeta_G(S) + \int U(S') K_G(S, S') dS' \\ &= \zeta_D(S) + \int U(S') K_D(S, S') dS. \end{aligned} \quad (10.133)$$

The latter half of this relation is an integral equation to be solved for  $U(S)$ . Once  $U(S)$  has been found, the problem for the marginal-sea tide is well posed. If the deep sea is, for example, idealized as an infinite half-plane ocean, then  $K_D(S, S')$  can be constructed by imposing the radiation condition far from the mouth. The boundary condition across the mouth for marginal sea tides, the specified mass flux  $U(S)$ , will thus incorporate radiative damping into the solution for marginal-sea tides. Garrett (1974) has discussed limiting cases of (10.133). Garrett and Greenberg (1977) have used the method to discuss possible perturbations of tides by construction of a tidal power station in the Bay of Fundy.

$U(S)$  as given by (10.133) is also the correct marginal-sea boundary condition for models of deep-ocean tides. Its application could allow optimal coupling of finely resolved marginal-sea models to more coarsely resolved global ones, but the methodology requires further development.

**Continental Shelf Tides** When the tide progresses parallel to a fairly long, straight continental shelf, then the free waves of section 10.4.6 are natural ones in terms of which to expect an economical representation of the tide. Munk, Snodgrass, and Wimbush (1970) analyzed California coastal tides in this way. In addition to the free waves capable of propagating energy at tidal frequencies, they introduced a forced wave to take local working by TGF into account. For the  $M_2$  tide, the Kelvin wave, the single representative member of the Poincaré continuum, and the forced wave have coastal amplitudes of 54, 16, and 4 cm, respectively. The coastal tide is dominated by the northward-propagating Kelvin mode, but further at sea the modes unexpectedly combine to yield an amphidrome (figure 10.27) whose existence was subsequently confirmed by Irish, Munk, and Snodgrass (1971). For the  $K_1$  California tide, the corresponding amplitudes are 21, 24, and 9 cm; the Kelvin wave is not nearly as important. Platzman (1979) has shown how this local representation is related to the properties of eigensolutions of LTE for the world ocean.

The California coast is too low in latitude for second-class shelf modes (section 10.4.6) to propagate energy at tidal frequencies. At higher latitudes, however, Cartwright (1969) has found evidence of their excitation; strong diurnal tidal currents without correspondingly great diurnal surface tides. At very low latitudes, low-mode edge waves could be resonant at tidal frequencies. Stock (private communication) has applied these ideas to the west coast of South America and to the Patagonian shelf. Geometrical difficulties prevent quantitative results in the latter case but the qualitative prediction that the coastally dominant Kelvin

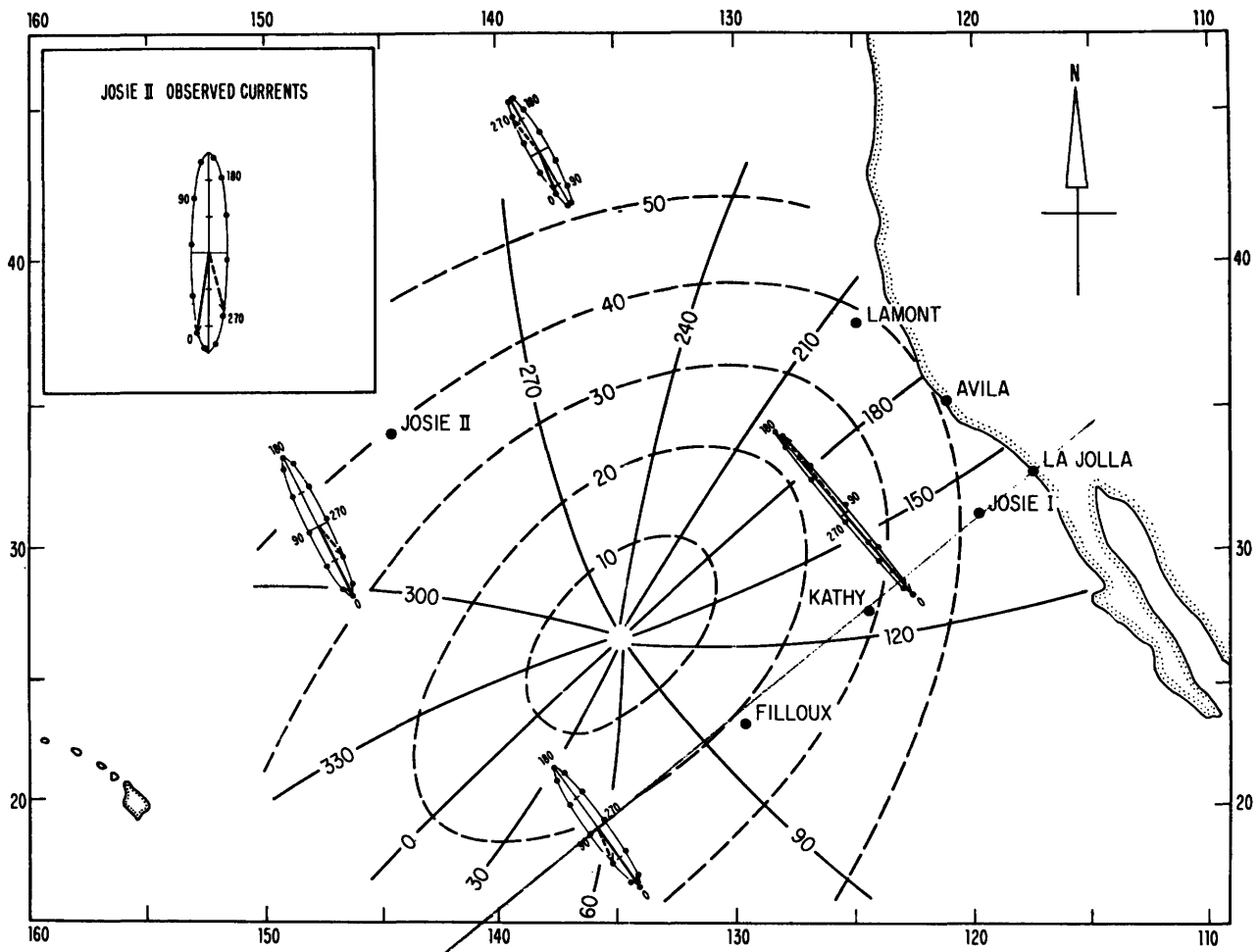


Figure 10.27  $M_2$  cotidal chart from Munk, Snodgrass, and Wimbush (1970) [amplitudes in cm, phases relative to moon's transit over Greenwich]. Ellipses show computed currents at ellipse center (ticks on ellipse axis correspond to  $1 \text{ cm s}^{-1}$ ).

Modal fit was to coastal stations plus Josie I, Kathy, and Filloux. Subsequent observations at Josie II confirmed phase shift across predicted amphidrome (Irish, Munk, and Snodgrass, 1971.)

mode decays by  $e^{-1}$  across the broad and shallow Patagonian shelf and that the low speed of long-wave propagation over the shallow shelf so compresses the length scale of the tides that a complex system of several amphidromes fits over the shelf are nonetheless important.

On all the shelves so far mentioned, the tide advances parallel to the shelf so that decomposition into modes traveling parallel to the coast is natural. But not all shelf tides are of this nature. Redfield (1958) has summarized observations of United States east coast continental shelf tides (figure 10.28). There the salient features are a very close correspondence between local shelf width and the coastal amplitude and phase of the tide. Tides are nearly coincident over the entire length and width (Beardsley et al., 1977) of the shelf, in marked contrast with the California case.

**Island Modification of Tides** Island tide records have been prized in working out the distribution of open-

ocean tides not only because of their open-ocean location but also because they have been supposed more representative of adjacent open-ocean tides than are coastal records.

Nevertheless, they are not entirely so. Tsunami travel-time charts suggest that tides in island lagoons may be delayed by as much as 20 minutes; harmonic constants for open-ocean tide charts correspondingly may need revision (Parke and Hendershott, 1980). Pelagic records (section 10.5.1) do not, of course, present this problem.

Diffraction effects near island chains may result in appreciable local modification of the tides. Larsen (1977) has studied the diffraction of an open-ocean plane wave of tidal frequency by an elliptical island (intended to model the Hawaiian Island plateau). A typical cotidal chart is shown in figure 10.29. Diffraction alters the time of high water by as much as an hour.

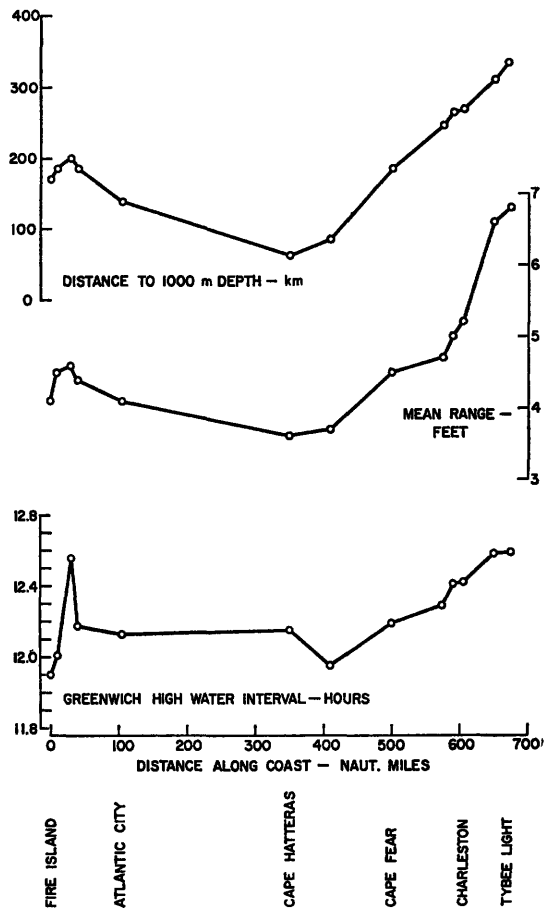


Figure 10.28 Distance from shore to 1000 m depth contour, mean coastal tidal range, and Greenwich high-water interval for selected outlying stations along the eastern coast of the United States. (Redfield, 1958.)

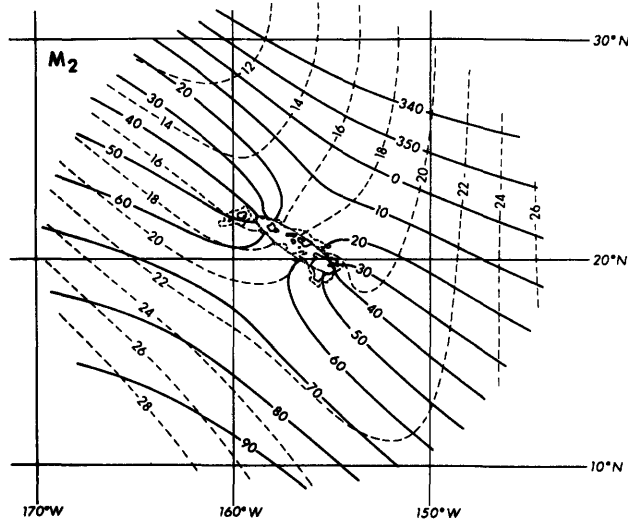


Figure 10.29 Theoretical cotidal chart for an  $M_2$  plane wave in a uniformly rotating ocean of 5000 m depth incident from the northeast on an elliptical island modeling the Hawaiian Chain. (Larsen, 1977.)

### 10.5.3 Global Tidal Models

The shape of the world's oceans is so complicated that realistic solutions of LTE must be numerical. Pioneering studies were made by Hansen (1949) and by Ros-siter (1958). The first global solution was presented by Pekeris and Dishon at the 1961 IUGG Assembly in Helsinki. I have reviewed subsequent developments elsewhere (Hendershott and Munk, 1970; Hendershott, 1973, 1977) and so will not attempt a comprehensive discussion.

Generally, numerical tidalists have solved (often by time-stepping) the forced LTE (10.5) with adjoined dissipative terms, and taking the numerical coasts as impermeable, or else they have solved the elliptic elevation equation [obtained by eliminating the velocities from LTE (10.5) without dissipative terms] for individual constituents (most often  $M_2$ ) with elevation at the numerical coast somehow specified from actual coastal observations. Combinations of these approaches have also been employed.

The first procedure yields solutions that may be thought of as a weighted sum of the dissipative analogs of Platzman's (1975) normal modes (section 10.4.8). Neither mass nor energy flows across the numerical coast. If the dissipation is modeled accurately (a matter of real concern since the smallest feasible global mesh spacing of about  $1^\circ$  cannot adequately resolve many marginal-sea and shelf tides), then such models should have fairly realistic admittances.

The second procedure attempts to circumvent this difficulty by allowing most or all dissipation to occur beyond the numerical coasts in regions that thus do not have to be resolved. It yields solutions that may be thought of as a tide reproducing the prescribed coastal tide plus a superposition of eigensolutions [of LTE (10.5) or of the elevation equation] that have vanishing elevation at the numerical coast. These eigensolutions have no simple oceanic counterparts since their coastal boundary condition does not require vanishing coastal normal velocity. The full solution satisfies the forced LTE and reproduces the prescribed coastal tide but also generally does not have vanishing normal velocity at the numerical coasts. Consequently there may be at any instant a net flow of water through the numerical coastline, and the flux of energy (averaged over a tidal period) through the numerical coastline need not be zero.

This flux of energy through the numerical coast is a realistic feature since the numerical coast is not intended to model the actual coast but, instead, crudely models the seaward edges of the world's marginal seas and shelves. The same is true of the mass flux, although, in using the solution to estimate ocean-tide perturbations of gravity, etc., the water that thus flows through the numerical coast must somehow be taken into account (Farrell, 1972b). Perhaps the greatest

drawback of the second procedure is the possibly resonant forcing of the unphysical zero-coastal-elevation eigensolutions. This can cause the model to have a very unrealistic admittance even though it is in principle capable of correctly reproducing all constituents. In practice, it often causes the model to be unrealistically sensitive to the way in which discretization of the equations or of the basin has been carried out. Thus Parke and Hendershott (1980) encountered resonances in solving for semidiurnal constituents by the second procedure and were forced to appeal to island observations in the manner described below in order to obtain realistic results. They encountered no similar resonances when solving for the diurnal  $K_1$  constituent, perhaps because the artificial coastal condition filters out the Kelvin-like modes that could be resonant at subinertial frequencies in the  $f$ -plane (section 10.4.2). All these remarks also apply to marginal-sea-tide models (section 10.5.2): when the elevation at the connection to the open ocean is specified *ab initio*.

These two procedures and variants of them have resulted in global solutions (most for  $M_2$ ) that show good qualitative agreement (Hendershott, 1973, 1977). The most recent published global models are by Zahel (1970), Parke and Hendershott (1980), and Accad and Pekeris (1978). I know of new calculations by Zahel, by Estes, and by Schwiderski (Parke, 1979) as well, but have not been able to examine them in detail. When all have been published, a careful comparison of these models with one another, with island and pelagic tidal data, with gravity data, and with tidal perturbations of satellite orbits ought to be carried out.

All the most recent solutions include effects of ocean loading and self-attraction (section 10.3). Many of them have been published since Cartwright (1977) and I (Hendershott, 1977) reviewed the tidal problem. The varying methods of solution may be summarized by abbreviating LTE (10.5) or the elevation equation as in Hendershott (1977):

$$\mathcal{L}[\zeta_0] = \mathcal{L}'[\iint G\zeta_0] + \mathcal{L}'[(1+k_2-h_2)U_2/g]. \quad (10.134)$$

Here  $U_2$  is the tide-generating potential (a second-order spherical harmonic) for a given constituent,  $(k_2, h_2)$  are Love numbers (section 10.3),  $\mathcal{L}$  and  $\mathcal{L}'$  are operators elliptic in space with  $\mathcal{L}$  representing LTE (10.5) or the elevation equation, and  $\iint G\zeta_0$  abbreviates the global convolution expressing effects of loading and self-attraction as in (10.14).

I attempted to solve (10.134) for  $M_2$  using the second procedure iteratively,

$$\mathcal{L}[\zeta_0^{(i+1)}] = \mathcal{L}'[\iint G\zeta_0^{(i)}] + \mathcal{L}'[(1+k_2-h_2)U_2/g], \quad (10.135)$$

(Hendershott, 1972) but the iteration did not look as though it would converge. Gordeev, Kagan, and Pol-

yakov (1977) found that inclusion of dissipation could result in convergence. Parke (1978) used the iterates  $\zeta_0^{(i)}$  as a basis set for a least-squares solution  $\hat{\zeta}_0$  of (10.134) of the form

$$\hat{\zeta}_0 = \sum A_i \zeta_0^{(i)} \quad (10.136)$$

in which the  $A_i$  are found by solving

$$\frac{\partial}{\partial A_i} \{E \equiv \iint_{\text{ocean}} \mathcal{L}(\hat{\zeta}_0) - \mathcal{L}'[\iint G\hat{\zeta}_0] - \mathcal{L}'[(1+k_2-h_2)U_2/g]^2\} = 0. \quad (10.137)$$

He obtained solutions that evidently were quite accurate [ $E$  as defined in (10.137) was small], but their realism was marred by the unphysical resonances of the second procedure. Parke and Hendershott (1980) therefore effectively adjusted the locations of these resonances to yield realistic global results by getting the  $A_i$  from a least-squares fit of (10.136) to island and pelagic observations.

Accad and Pekeris (1978) noticed that  $\iint G\zeta_0^{(i)}$  was very similar to  $\zeta_0^{(i+1)}$ . They therefore put

$$\iint G\zeta_0^{(i)} = K\zeta_0^{(i)} + \iint \Delta\zeta_0^{(i)}, \quad (10.138)$$

where  $K$  is a constant evaluated empirically at each iteration by

$$K = \iint [\zeta_0^{(i)*} \iint G\zeta_0^{(i)}] / \iint [\zeta_0^{(i)*} \zeta_0^{(i)}] \quad (10.139)$$

and then iterated not (10.135) but

$$\begin{aligned} & \mathcal{L}[\zeta_0^{(i+1)}] - K \mathcal{L}'[\zeta_0^{(i+1)}] \\ & = \mathcal{L}'[\iint \Delta\zeta_0^{(i)}] + \mathcal{L}'[(1+k_2-h_2)U_2/g]. \end{aligned} \quad (10.140)$$

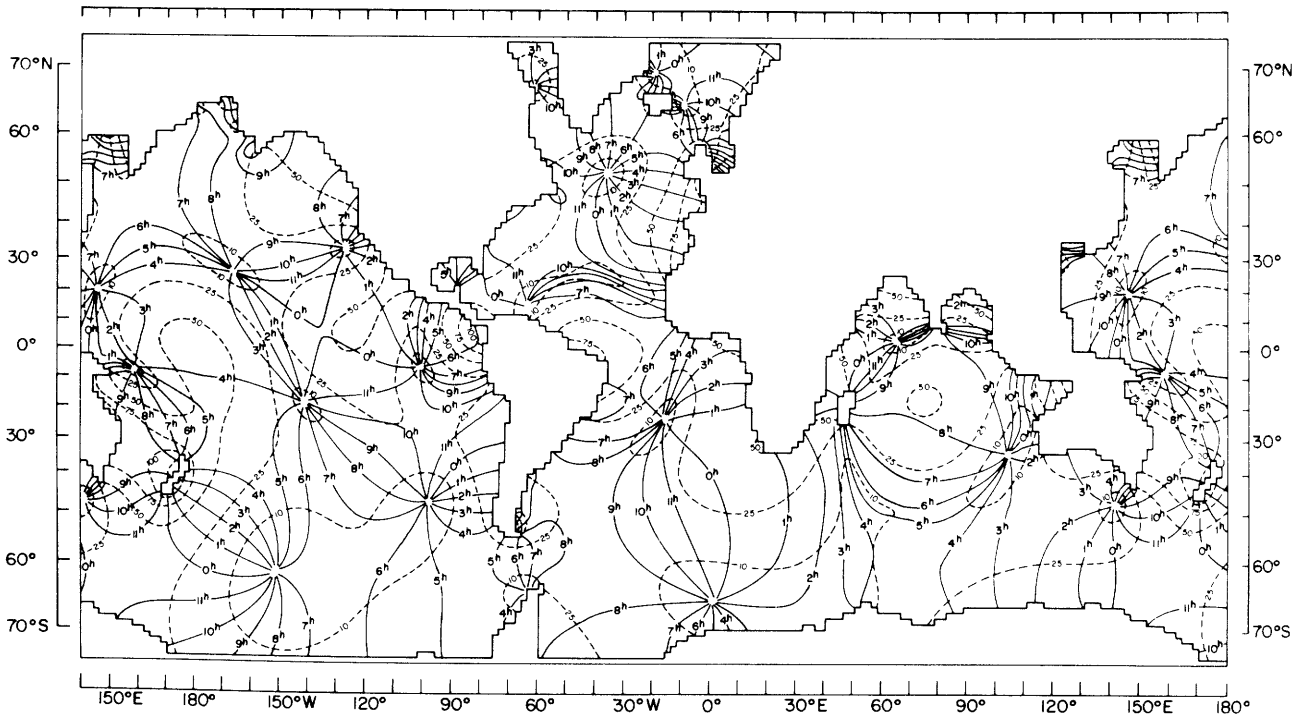
This greatly accelerated the slow convergence of (10.135), presumably already established by dissipation in their calculations.

Figure 10.30 shows two  $M_2$  global cotidal maps of Accad and Pekeris (1978), which differ only in the inclusion of the convolution terms  $\iint G\zeta_0$ . These terms do not result in an order of magnitude alteration of the computed tide but their effects are large enough that they must be included in any dynamically consistent model aiming at more than order-of-magnitude correctness. These solutions and others like them are obtained solely from a knowledge of the tidal potential and are, in that sense, as close as modern investigators have come to attaining Laplace's original goal.

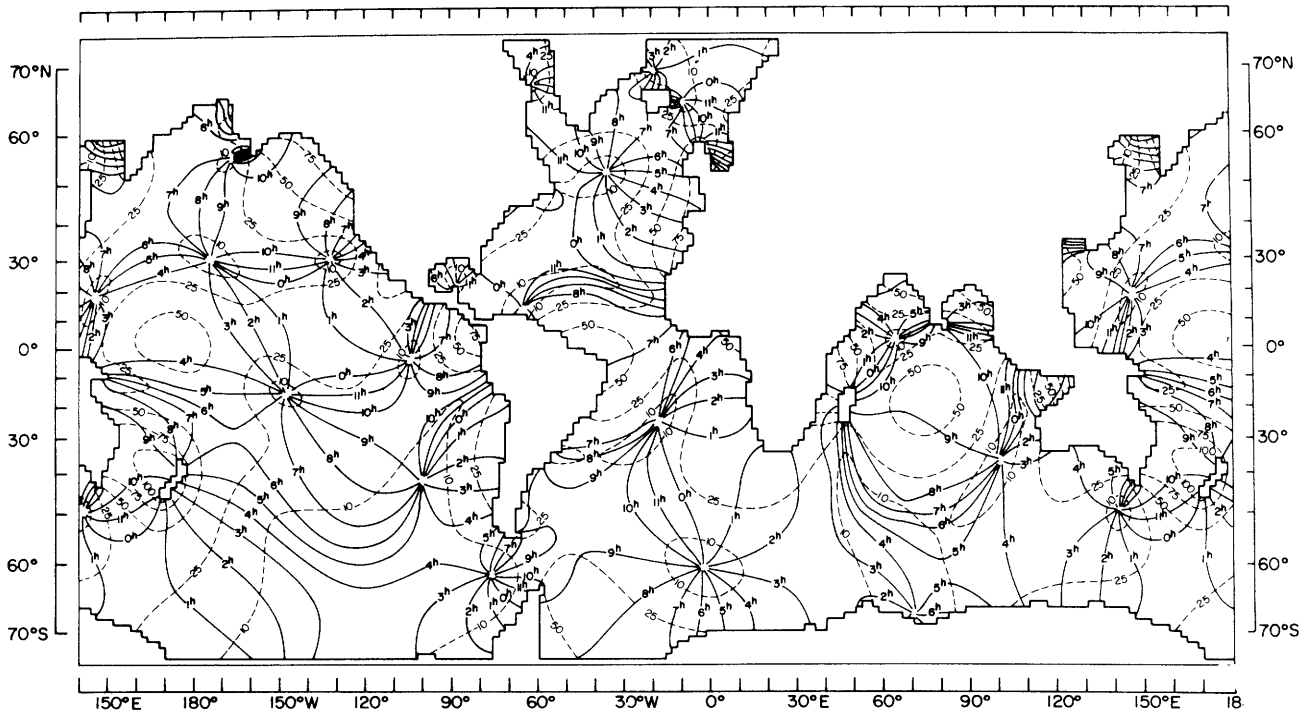
## 10.6 Internal Tides

### 10.6.1 Introduction

Internal tides have long been recognized as internal waves somehow excited at or near tidal periods. Their potential as a source of error in hydrographic casts seems to have been recognized since their earliest re-



(10.30A)



(10.30B)

Figure 10.30 Two theoretical calculations of the global  $M_2$  tide obtained solely from a knowledge of the astronomical tide-generating forces (A) and differing only in the inclusion (B) of the effects of loading and self-attraction. (Accad and Pekeris, 1978.)

ported observation by Nansen (1902). Because constant-depth internal-wave modes are almost orthogonal to the ATGF (they would be completely so if the sea surface were rigid and the ATGF exactly depth independent) it has always been difficult to see why internal tides exist at all. The work of Zeilon (1911, 1912) appears to be the precursor of the now generally accepted explanation—energy is scattered from surface to internal tides by bottom roughness—but there has been a history of controversy. The lack of correlation between internal tides at points separated vertically by  $O(100 \text{ m})$  or horizontally by  $O(100 \text{ km})$  puzzled early observers. Subsequent observations showed semidiurnal and diurnal internal tides to be narrow-band processes each with a finite band width  $\Delta\sigma$  of order several cycles per month. This property manifests itself both in a decay of spatial coherence of internal tides over a length associated with the spread of spatial wavenumbers corresponding to  $\Delta\sigma$  and in temporal intermittency over times  $\Delta\sigma^{-1}$ , as well as in a corresponding lack of coherence with either the surface tide or the ATGF. Typical observations are shown in figure 10.31.

### 10.6.2 Generation Mechanisms

Zeilon (1934) carried out laboratory experiments showing that a step in bottom relief could excite internal waves in a two-layer fluid when a surface tidal wave passed overhead. Two-layer models are attractive analytically because each layer is governed by a well-posed boundary-value problem; such experiments have been studied theoretically by Rattray (1960) and many others.

Haurwitz (1950) and Defant (1950) noticed that in the  $f$ -plane both the horizontal wavelength and the phase speed of plane internal waves grow very large as  $\sigma \rightarrow f_0$  [(10.23e) with  $D_* = D_n$ ]. Resonance with the ATGF might thus be possible near the inertial latitudes corresponding to tidal frequencies. But the equatorial  $\beta$ -plane solutions (section 10.4.5) (even though only qualitatively applicable at tidal inertial latitudes) show that this apparent possibility of resonance is an artifact of the  $f$ -plane, which provides WKB solutions of LTE, and so cannot be applied at the inertial latitudes.

Miles (1974a) has shown that the Coriolis terms customarily neglected in the traditional approximation scatter barotropic energy into baroclinic modes (section 10.3). Observations of internal tides (section 10.6.3) appear to favor bottom relief as the primary scatterer, but this may be because steep bottom relief is spatially localized whereas the “extra” Coriolis terms are smoothly distributed over the globe. Further theoretical work is needed to suggest more informative observations.

For a continuously stratified ocean, Cox and Sandstrom (1962) calculated the rate of energy flow from

surface to internal tides due to single scattering from small-amplitude, uniformly distributed, open-ocean-bottom roughness  $\epsilon D_1(x, y)$  [where  $\epsilon \ll 1$ ,  $D_1$  is  $O(1)$ ]. Their calculation is most succinctly summarized by specializing to one-dimensional relief  $D_1(x)$  and constant buoyancy frequency  $N_0$ . If the incident surface tidal-velocity field is idealized as  $U \exp(-i\sigma t)$ , with no space dependence, then the singly scattered internal-tide field  $w^{(1)}$  is obtained by solving (10.45)

$$\frac{\partial^2 w^{(1)}}{\partial z^2} - \left( \frac{N_0^2}{\sigma_T^2 - f_0^2} \right) \frac{\partial^2 w^{(1)}}{\partial x^2} = 0 \quad (10.141)$$

and

$$\frac{\partial w^{(1)}}{\partial x} + \frac{\partial w^{(1)}}{\partial z} = 0 \quad (10.142)$$

subject to

$$w^{(1)} = 0 \quad \text{at } z = 0, \quad (10.143)$$

$$w^{(1)} = \epsilon U \partial D_1 / \partial x \quad \text{at } z = -(D_* + \epsilon D_1) \quad (10.144)$$

plus a radiation condition as  $|x| \rightarrow \infty$ .

Equation (10.143) idealizes the free surface as rigid (adequate for internal waves); (10.144) is the  $O(\epsilon)$  expansion about the mean relief  $z = -D_*$  of the condition (10.15) of zero normal flow at the actual relief:

$$w = u \frac{\partial}{\partial x} (D_* + \epsilon D_1) \quad \text{at } z = -D_* - \epsilon D_1. \quad (10.145)$$

The solution of (10.141)–(10.144) for  $w^{(1)}$  is

$$w_1(x, z) = \int_{-\infty}^{\infty} \bar{w}_1(l, z) \exp(ilx) dl, \quad (10.146)$$

where

$$\bar{w}_1(l, z) = \frac{\overline{(\epsilon U \partial D_1 / \partial x)}}{\sin[-l D_* N_0 / (\sigma_T^2 - f_0^2)^{1/2}]} \quad (10.147)$$

with  $\overline{(\epsilon U \partial D_1 / \partial x)}$  defined as the Fourier transform of  $(\epsilon U \partial D_1 / \partial x)$ . The integrand of (10.14.6) has simple poles at  $[-l D_* N_0 / (\sigma_T^2 - f_0^2)^{1/2}] = n\pi$ , i.e., at horizontal wavenumbers  $l$  satisfying the internal wave dispersion relation  $\sigma_T^2 - f_0^2 = g D_n l^2$ ,  $D_n = N_0^2 D_*^2 / g n^2 \pi^2$ . Equatorward of the tidal inertial latitude,  $\sigma_T^2 < f_0^2$ , so that each pole is real and corresponds to an internal wave traveling away from the scattering relief. Poleward of the tidal inertial latitude,  $\sigma_T^2 > f_0^2$ , so that each pole is imaginary and the corresponding internal mode decays exponentially away from the scattering roughness without carrying energy away. The sum of all evanescent modes also decays in the vertical away from the scattering relief. Wunsch (1975) reports the existence of observations showing this evanescent behavior for diurnal internal tides.

When  $\sigma_T^2 > f_0^2$ , (10.141) is hyperbolic in  $(x, t)$  with characteristic slope  $(\sigma_T^2 - f_0^2)^{1/2} / N_0$ . Baines (1971) solved

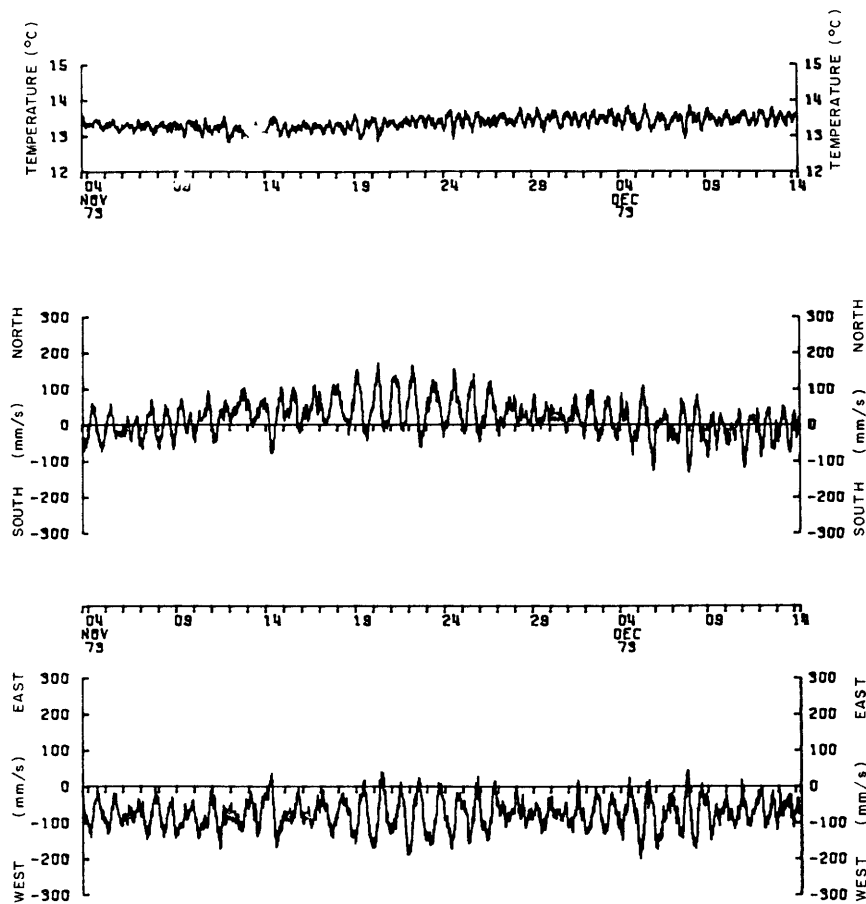


Figure 10.31A Time series of temperature and velocity at the IWEX mooring (Hatteras Abyssal Plain) at 640 m depth (Briscoe, 1975b).

(10.141) and (10.145) exactly, by the method of characteristics, thus eliminating the restriction to weakly sloping relief. The analytical novelty of his work was the imposition of the radiation condition on the characteristic form

$$F(x - Rz) + G(x + Rz), \quad R = N_0 / (\sigma_T^2 - f_0^2)^{1/2}$$

of the solutions of (10.141) by, for example, choosing

$$F(x) = \int_0^\infty e^{ix} \overline{F(l)} dl$$

so that  $F(x \pm Rz) \exp(-i\sigma_T t)$  contains only outgoing plane waves. Laboratory work (Sandstrom, 1969) and analysis (Wunsch, 1969) showed that when bottom and tidal characteristic slopes coincide, the near-bottom motion is strongly intensified. Wunsch and Hendry (1972) show evidence for such intensification over the continental slope south of Cape Cod (figure 10.32).

The general possibility that diurnal tides enhance diurnal inertial motion by some mechanism has been suggested by Ekman (1931), Reid (1962) and Knauss (1962b). I (Hendershott, 1973) estimated the amplitude of motion if the mechanism is scattering of surface

tides into internal tides by open-ocean bottom roughness, but obtained a result sufficiently small that it would not stand out noticeably against the high level of inertial motion found at all mid-latitudes (Munk and Phillips, 1968).

Thus far, the discussion is in terms of linearly scattered linear waves. Bell (1975) considers the formation of internal lee waves on periodically varying barotropic tidal currents. This process could generate a complex spectrum of internal waves even with a monochromatic surface tide. What actually occurs when laboratory or ocean stratified flow passes over relief is complicated. In Massachusetts Bay, Halpern (1971) has observed that tidal flow over a ridge generates a thermal front that propagates away as a highly nonlinear internal wavetrain (Lee and Beardsley, 1974) or as an internal bore. Such bores are commonly observed along the Southern California coast (Winant, 1979).

Maxworthy (1979) emphasizes the importance of the collapse of the stirred region that initially develops over relief in the subsequent generation of laboratory internal waves. The relative importance of all these processes near the sea floor is unknown. If separation

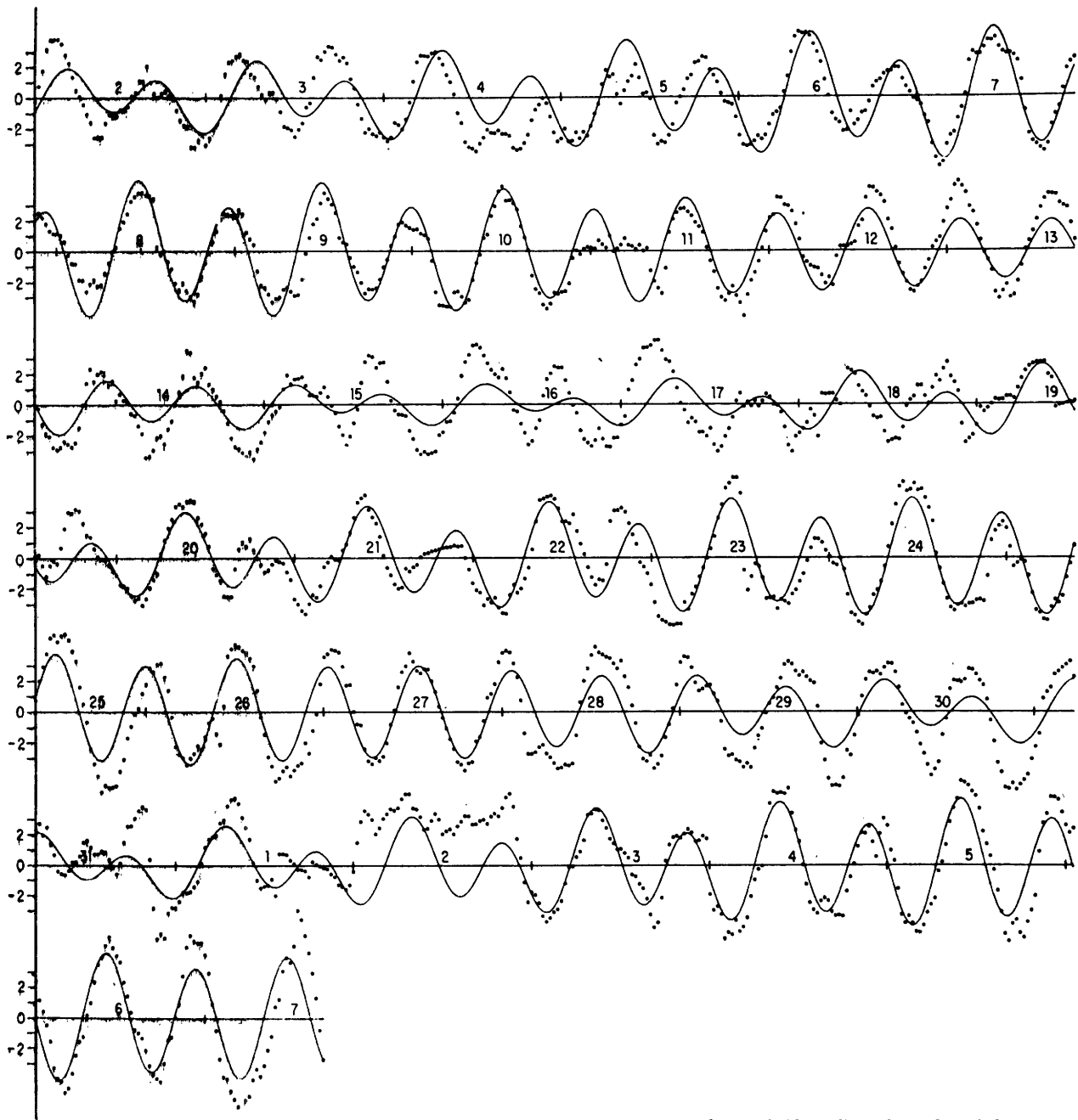


Figure 10.31B Observed (dotted) and predicted barotropic (solid) longshore bottom velocity at Josie I (figure 10.27) off the southern California coast. (Munk, Snodgrass, and Wimbush, 1970.)

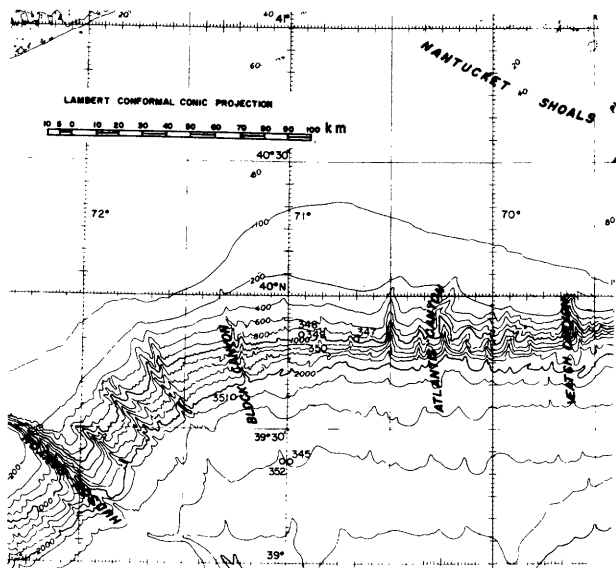


Figure 10.32A Current meter mooring positions and shelf topography. (Wunsch and Hendry, 1972.)

over abyssal relief does occur in tidal currents, it could contribute to abyssal mixing by helping to form the near-bottom laminae observed by Armi and Millard (1976). Wunsch (1970) made a somewhat similar suggestion based on laboratory studies.

Besides this potential complexity of generation, the medium through which the internal tide moves is strongly inhomogeneous in space and time. The overall result is the complicated and irregularly fluctuating internal tide observed. Still, away from generation regions, some features of the linear theory shine through.

### 10.6.3 Observations

In linear theory, breaks in the slope of the relief and extended regions where that slope coincides with a tidal characteristic slope make themselves felt in the body of the ocean as narrow-beam disturbances concentrated along the characteristics (Rattray et al., 1969). The beams are typically narrow (figure 10.33) and their (characteristic) slope in the presence of mean currents varies both with local stratification and shear. This suggests that, especially near generation regions, the internal tide will have a complex spatial structure and that its amplitude at a given point may vary markedly as nearby stratification and mean flow change. Thus Hayes and Halpern (1976) document very large variability of semidiurnal internal tidal currents during a coastal upwelling event; they account for much of it by appealing to the deformation of characteristics as vertical and horizontal density gradients change during the upwelling. Regal and Wunsch (1973) find internal tidal currents at site D, over the continental slope south of Cape Cod, to be concentrated near the surface and there highly (and uncharacteristically) coherent

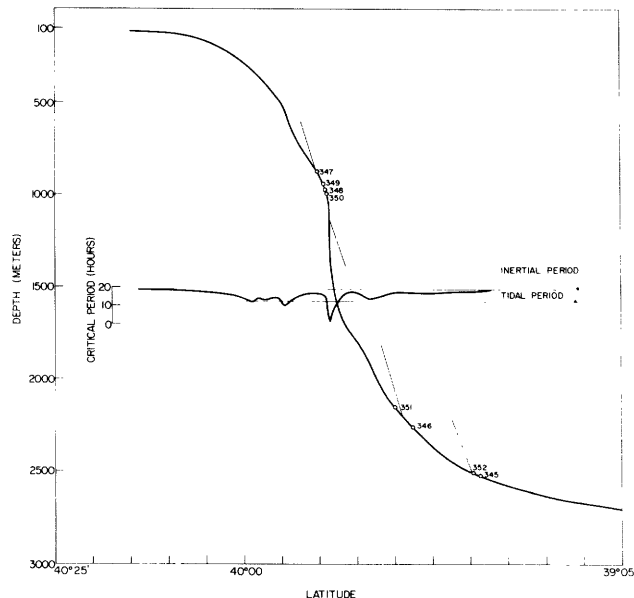


Figure 10.32B Profile of topography through the array along the dashed line of figure 10.32A with mooring positions indicated. Several internal wave characteristics for the  $M_2$  tide are shown, and the critical period (at which internal-wave characteristics are locally tangent to the relief) is plotted across the profile. (Wunsch and Hendry, 1972.)

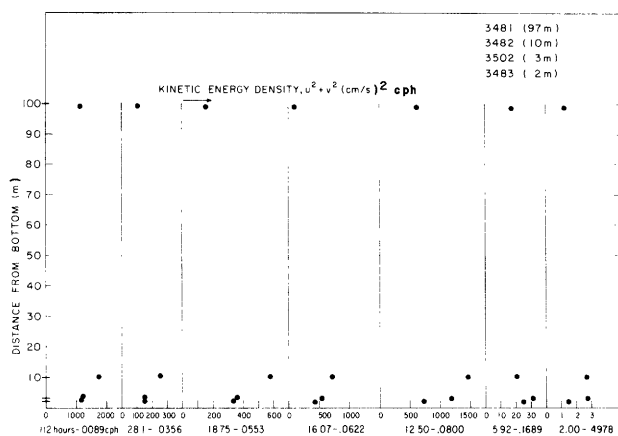


Figure 10.32C Vertical profiles of kinetic energy density (observed values are solid dots) for various periods over the slope where the tidal characteristic is locally tangent to the relief (moorings 347-350). (Wunsch and Hendry, 1972.)

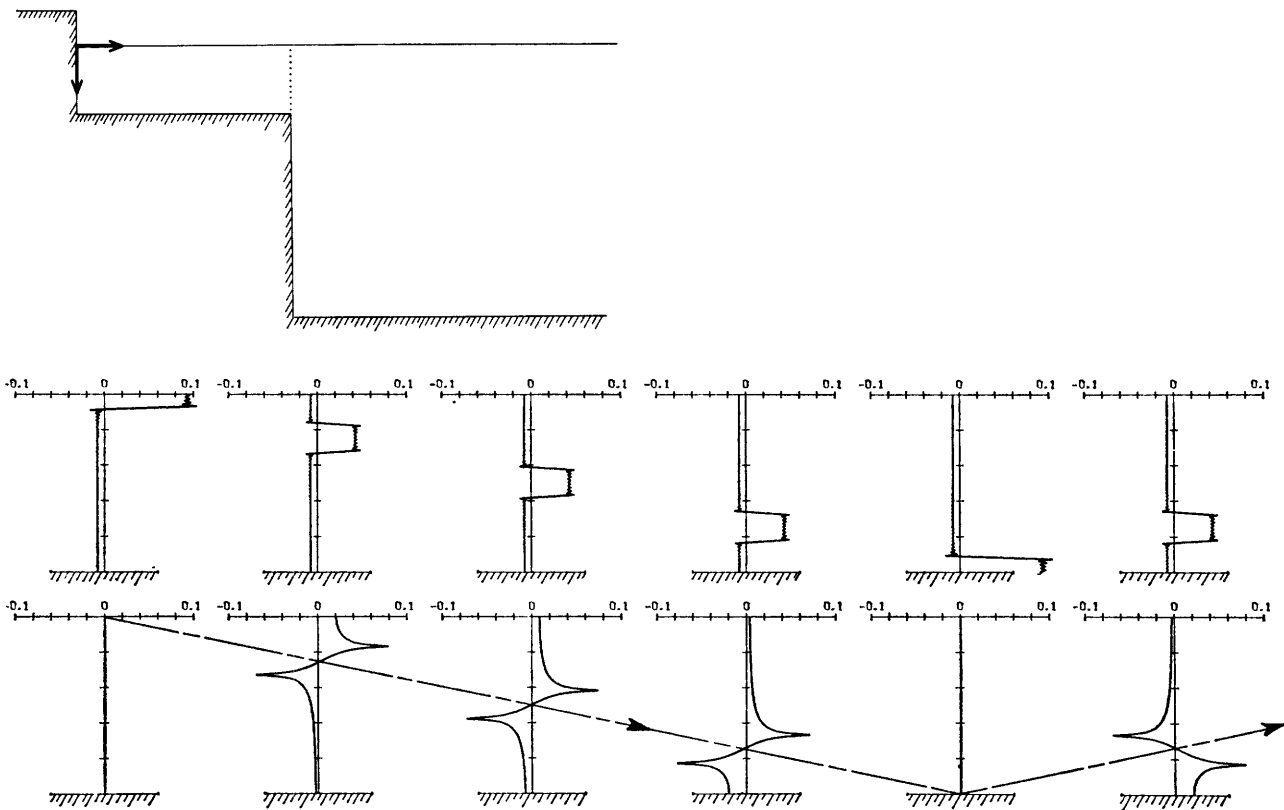


Figure 10.33 Depth distribution of horizontal internal tidal currents away from a step shelf (top) at two times (center and bottom) separated by a quarter-wave period. Ratio of deep sea to shelf depth is 12.5, characteristic slope is 1/715; current

profiles begin at shelf edge and are separated horizontally by 1.8 of the deep-sea (first-mode) internal-tide wavelength. (Ratray et al., 1969.)

with the surface tide. The result is consistent with generation where tidal characteristics graze the slope perhaps 60 km to the north followed by propagation along characteristics that leave the region of tangency and bounce once off the ocean floor before passing through the near surface part of the water column at site D (figure 10.34). Observations at site L, some 500 km to the south, show no evidence of propagation along beams.

Beams are a coherent sum of many high internal modes. We intuitively expect that high modes are more rapidly degraded by whatever processes ultimately lead to dissipation than are low modes, and that they are more sensitive to medium motion and fluctuation than are low modes because they propagate so slowly. We thus do not expect beamlike features in the deep sea, and they are not observed. Instead, we expect a few low modes to dominate in a combination of arrivals from distant steep relief. These will have made their way through significant oceanic density fluctuations and through fluctuations of mean flows often at an appreciable fraction of internal-wave-phase speeds. The line spectrum characteristic of the ATGF and the surface tide will thus be so broadly smeared into semidiurnal and diurnal peaks that individual constituents or

even the spring-neap cycle are at best very difficult (Hecht and Hughes, 1971) to perceive.

The most complete description of open-ocean internal tides is due to Hendry (1977), who used the western central Atlantic Mid-Ocean Dynamics Experiment (MODE) data. Figure 10.35 summarizes the results.  $M_2$  tends to dominate semidiurnal temperature variance over the water column. Adjacent  $N_2$  and  $S_2$  variances are nearly equal, and the vertical variation of  $N_2$ ,  $S_2$  variance generally follows  $M_2$  (with qualifications near the bottom).  $M_2$  likewise dominates horizontal semidiurnal current variance over the water column. At subthermocline depths  $M_2$  variance approaches estimates of the barotropic  $M_2$  tidal current variance while  $S_2$  and  $N_2$  variances exceed their barotropic counterparts by an order of magnitude. All this suggests that much of what appears in the  $N_2$  and  $S_2$  bands has really been smeared out of  $M_2$ . The vertical distribution of variance is broader than the two WKB profiles  $(\partial\bar{\theta}/\partial z)^2 N(z)^{-1}$  ( $\bar{\theta}$  is mean potential temperature) and  $N(z)$ , for temperature and horizontal current variance, respectively. This indicates that the lowest vertical modes dominate.  $M_2$  temperature variance has a coherence of about 0.7 with the ATGF in the upper thermocline while  $N_2$  and  $S_2$  are far less coherent with the

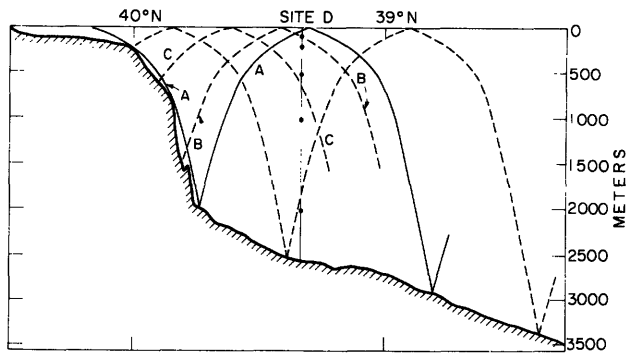


Figure 10.34A Profile of relief along 70°W (see figure 10.32 for local isobaths) together with selected semidiurnal characteristics passing near site D. (Regal and Wunsch, 1973.)

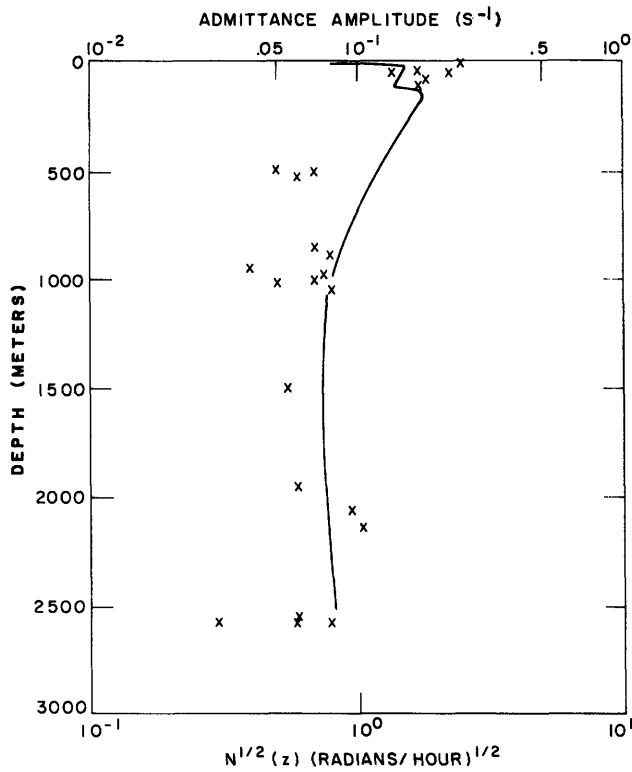


Figure 10.34B Admittance amplitude  $x$  for semidiurnal tidal currents together with buoyancy frequency  $N(z)$  at site D. Near-surface admittances are strongly intensified; currents there are highly coherent with the surface tide. (Regal and Wunsch, 1973.)

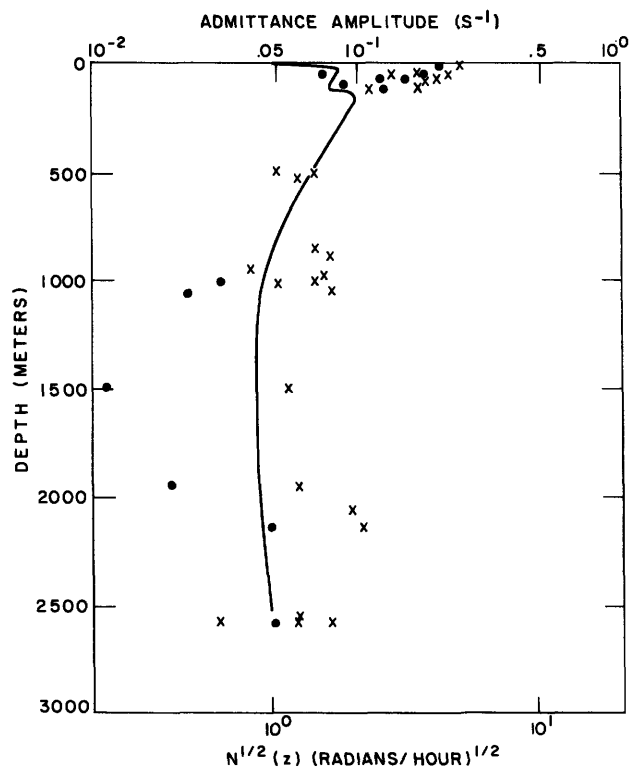


Figure 10.34C A similar display at site L, 599 km south of site D, shows no comparable surface intensification. (Regal and Wunsch, 1973.)

ATGF but yet not totally incoherent. The  $M_2$  first internal mode dominates and propagates to the southeast; this plus the (significantly not random) phase lag between  $M_2$  and  $S_2$  in the thermocline (the age of the internal tide) point to the 700-km distant Blake escarpment as a generating region. Other discussions of open-ocean internal tides are consistent with the foregoing picture although necessarily based upon less extensive observations.

Wunsch (1975) reviews observations allowing estimation of the energy density (in units of ergs per squared centimeters) of internal tides and suggests that it is from 10 to 50% of the corresponding energy density of the barotropic tide, albeit with wide and unsystematic geographic variation.

#### 10.6.4 Internal Tides and the Tidal Energy Budget

It thus appears that barotropic tides somehow give up energy to internal tides. Return scattering is probably unimportant. It is important to know the rate at which this energy transfer occurs because (section 10.5) the energy budget for global tides may not yet be closed. Wunsch (1975) reviews estimates arising from the various scattering theories outlined above (section 10.6.2); typical values are  $0.5 \times 10^{19}$  ergs $^{-1}$  from deep-sea roughness [using the theory of Cox and Sandstrom as rediscussed by Munk (1966)],  $6 \times 10^7$  erg cm s $^{-1}$  from continental shelves [using the theory of Baines (1974) and also from independent measurements by Wunsch and Hendry (1972)]. The latter value extrapolates to  $5.6 \times 10^{15}$  ergs $^{-1}$  over the globe.

A bound on this estimate independent of scattering theories was pointed out by Wunsch (1975). Internal-tide energy densities  $E_I$  are order 0.1 to 0.5 times surface-tide energy densities  $E_S$ . Group velocities  $c_{gt}$  of internal waves are order  $(D_n D_0)^{1/2} \approx (N^2 D_0 / g n^2 \pi^2)^{1/2}$  times group velocities  $c_{gs}$  of long-surface gravity waves. If open-ocean tidal energy is radiated toward shallow seas (or any other dissipation region) at rates  $c_{gt} E_S$  and  $c_{gt} E_I$ , then internal tides can never account for more than  $O(10\%)$  of the total energy lost from surface tides.

Wunsch's (1975) discussion of the caveats to this result has not been substantially altered by subsequent developments. Nonlinear interactions that drain internal energy from the tidal bands to other frequencies and scales certainly do occur but their rates are not yet accurately estimable. Such rates as have been calculated [Garrett and Munk (1972a) calculated the energy loss due to internal wave breaking; McComas and Bretherton (1977) the time scale for the low-frequency part of the internal wave spectrum to evolve by resonant interactions]; they are small, but the problem is not closed.

#### 10.6.5 Internal Tides and Ocean Stirring

Even if internal tides turn out to be a minor component of the global tidal-energy budget, they could be an im-

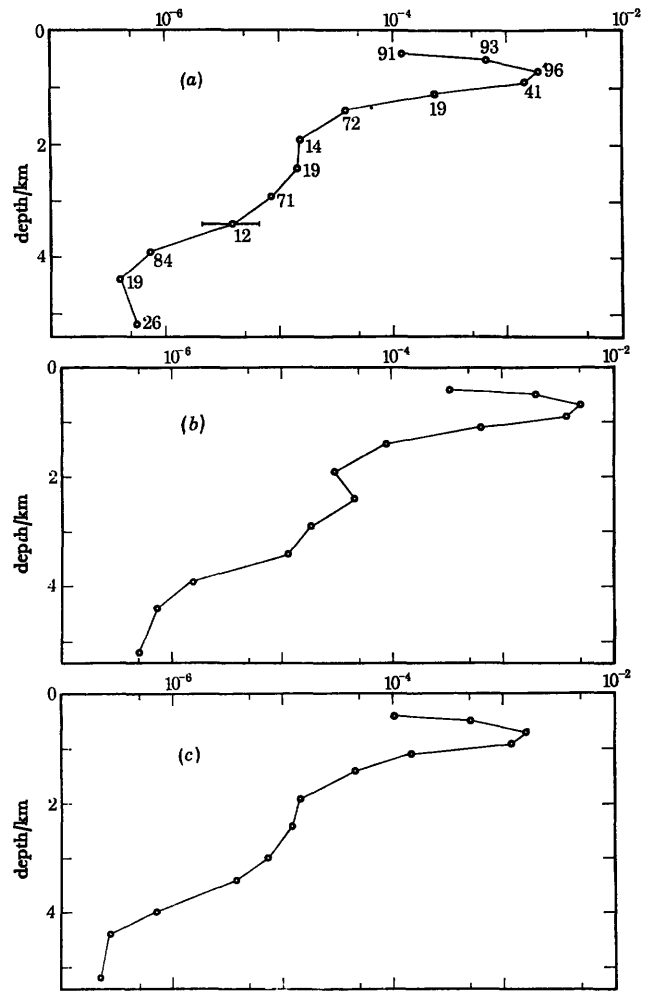


Figure 10.35A Vertical profile of squared temperature fluctuations in the (a)  $S_2$  band ( $^{\circ}\text{C}$ ), averaged at depth levels over the entire array; the number of 15-day-piece lengths at each level is indicated. Vertical profile of average squared temperature fluctuations in the (b)  $M_2$  band. Vertical profile of average squared temperature fluctuations in the (c)  $N_2$  band. (Hendry, 1977.)

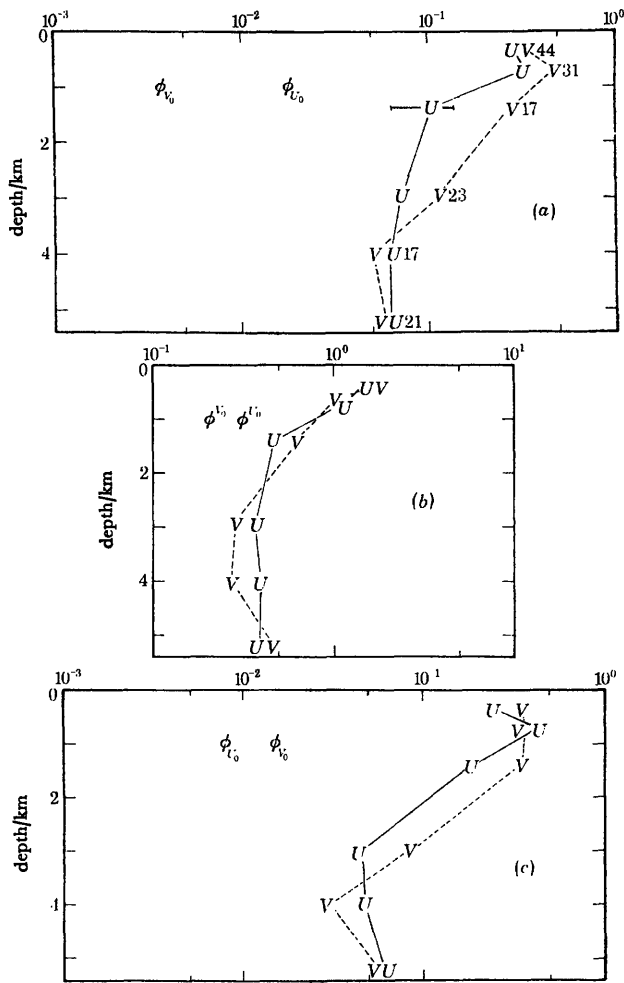


Figure 10.35B Vertical profile of squared horizontal current ( $\text{cm s}^{-1}$ ) for  $U$  (east) and  $V$  (north) in the (a)  $S_2$  band, averaged at depth levels over the entire array; estimates of squared amplitude for the barotropic current components  $U$  and  $V$  are given, showing that the currents are dominated by internal waves at all depths. Similar estimates for the (b)  $M_2$  band currents. Here the deep currents are greatly influenced by the barotropic mode. Similar estimates are given for the (c)  $N_2$  band; internal waves appear to dominate at all depths. (Hendry, 1977.)

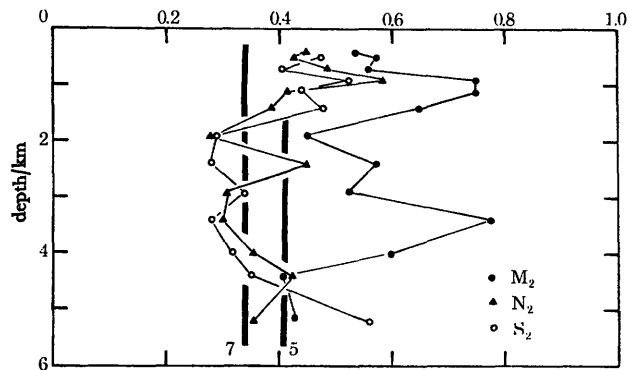


Figure 10.35C Vertical profile of average coherence amplitude of temperature fluctuations and the equilibrium tide for three semidiurnal frequency bands. The averages are taken over the whole array at depth levels, and include individual cases with both five and seven degrees of freedom. The expected values of coherence amplitude for zero true coherence are shown for each case, and while the central  $M_2$  band shows a definite determinism, the adjacent frequency bands are much more dominated by randomly phased temperature fluctuations. (Hendry, 1977.)

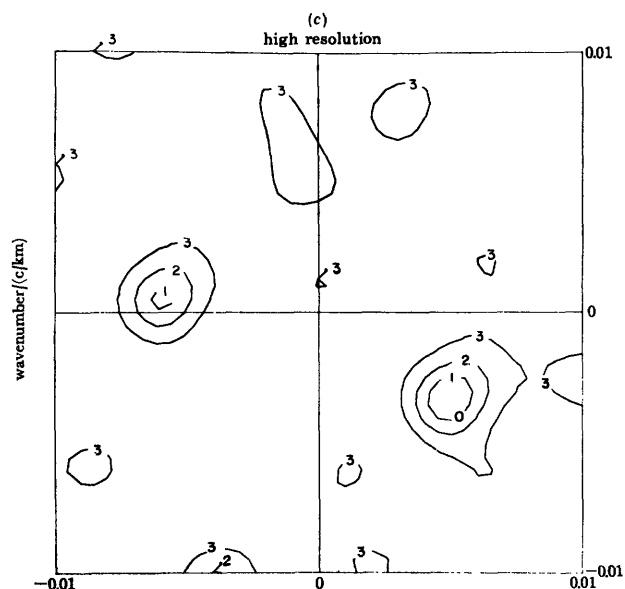


Figure 10.35D Conventional wavenumber spectrum of first-mode  $M_2$  temperature fluctuations from MODE. The peak in the southeast quadrant has wavenumber  $1/163$   $\text{cpkm}$  and represents a wave propagating from northwest to southeast. A secondary peak in the northwest quadrant is interpreted as an alias of the main peak. (Hendry, 1977.)

portant source of energy for ocean stirring and mixing. About 10% of the total tidal dissipation would be energetically adequate (Munk, 1966). The hypothesis is that internal tides somehow (by bottom turbulence, by nonlinear cascade) cause or enhance observed fine structure and microstructure events in which mixing is believed to be occurring. It thus is pertinent to examine observations for any correlation between tidal phenomena and smaller-scale events. Such a correlation could be temporal [with the intensity of small structure modulated at semidiurnal, diurnal, fortnightly (i.e., the spring-spring interval) or even longer tidal periods] or spatial (with small structure near generators different from that far away).

Although definitive studies have yet to be made, preliminary indications are that little such correlation exists. Cairns and Williams (1976) contour the spectrum of vertical displacement in a frequency-time plane for 17 days over the frequency band 0.2–6.0 cpd (figure 10.36) but see no modulation at tidal or fortnightly periods of any part of the spectrum. Wunsch (1976) finds no correlation between the overall spectral level of internal waves (specifically, the spectral intensity at 5-hour period of a model fitted to observed spectra) and the intensity of the internal tidal peak for observations from the western North Atlantic (figure 10.37).

The demonstration that tidal contributions to ocean mixing are significant will thus involve subtle measurements. Perhaps something may be learned by comparing internal waves, fine structure, and microstructure in the open ocean with their counterparts in the relatively tideless Mediterranean Sea or in the Great Lakes (see chapters 8 and 9).

### 10.7 Tidal Studies and the Rest of Oceanography

Although tidal studies were the first dynamic investigation of oceanic response to forcing, insight into wind- and thermohaline-driven ocean circulation developed largely independently of them. In the case of semidiurnal and diurnal tides, the reason is primarily dynamic. But the dynamics of long-period tides are likely to be much more like those of the wind-driven circulation (both steady and transient) than like those of semidiurnal and diurnal tides. It is possible that, if the long-period components of the ATGF had been large enough to make the long-period tides stand out recognizably above the low-frequency noise continuum, then the early tidalists might have recognized, in the low-frequency tides, features such as westward intensification also evident in the general circulation. They might then have been forced into the recognition that a linear superposition of (possibly damped) first-class waves could not account for long-period tides, as it seems able to do for semidiurnal and diurnal tides. As

things are, however, long-period tides are so near to the noise level that their observation did not provide a global picture clear enough to force tidalists out of the semidiurnal-diurnal framework.

It was, in fact, insight into the problem of time-dependent wind-driven ocean circulation that led Wunsch (1967) to provide the modern view of long-period tides: a superposition of damped second-class waves (section 10.4.4) whose horizontal length scales are only  $O(10^3 \text{ km})$  and whose amplitudes and phases are likely to undergo substantial fluctuations in time on account of the overall time variability of the ocean currents through which they propagate. Laplace had supposed that a small amount of dissipation would bring the long-period tides into equilibrium, i.e., the geocentric sea surface  $\zeta$  would be an equipotential of the total tide-generating potential  $\Gamma$  (Lamb, 1932, §217). The most recent elaboration of this view is by Agnew and Farrell (1978), who solved the integral equation

$$\zeta = \zeta_0 + \delta = \Gamma/g$$

[with  $\delta$  (the solid-earth tide) and  $\Gamma$  given by (10.11) and (10.12) as functions both of the observed tide  $\zeta_0$  and of the long-period astronomical potential  $U_2$ ] for equilibrium global-ocean fortnightly and monthly tides  $\zeta_0$  subject to the conservation of mass. Wunsch's (1967) analysis and dynamic model of the fortnightly tides suggest that they are not in equilibrium with either the astronomical potential  $U_2$  or with the full potential  $\Gamma$  of Agnew and Farrell (1978). Their Pacific averaged admittance has magnitude  $0.69 \pm 0.02$  relative to  $\Gamma$  with significant island-to-island variation. The Pacific averaged monthly tide admittance has magnitude  $0.90 \pm 0.05$  relative to  $\Gamma$ , but island-to-island fluctuations vanish only by pushing individual island admittances to the very end of their error bands. Whether the kinds of dissipation and of nonlinear interaction between low-frequency motions that occur in the real ocean favor an equilibrium tidal response at sufficiently low frequencies is not yet known either observationally or theoretically. The 14-month pole tide is known to be significantly non-equilibrium in the shallow seas of Northern Europe (Miller and Wunsch, 1973) but nearly invisible elsewhere.

Observations of long-period tides have thus been too noisy to exert real influence on tidal studies and hence on dynamic oceanography. But the theoretical ideas emerging from study of the low-frequency solutions of LTE have been of great importance for dynamic oceanography (even though they are likely to be inadequate to model the full dynamics of the general circulation).

Steady (as opposed to wavelike) solutions of LTE obtained by active tidalists (Hough, 1897; Goldsbrough, 1933) had a profound effect on dynamic oceanography through the review by Stommel (1957b) of

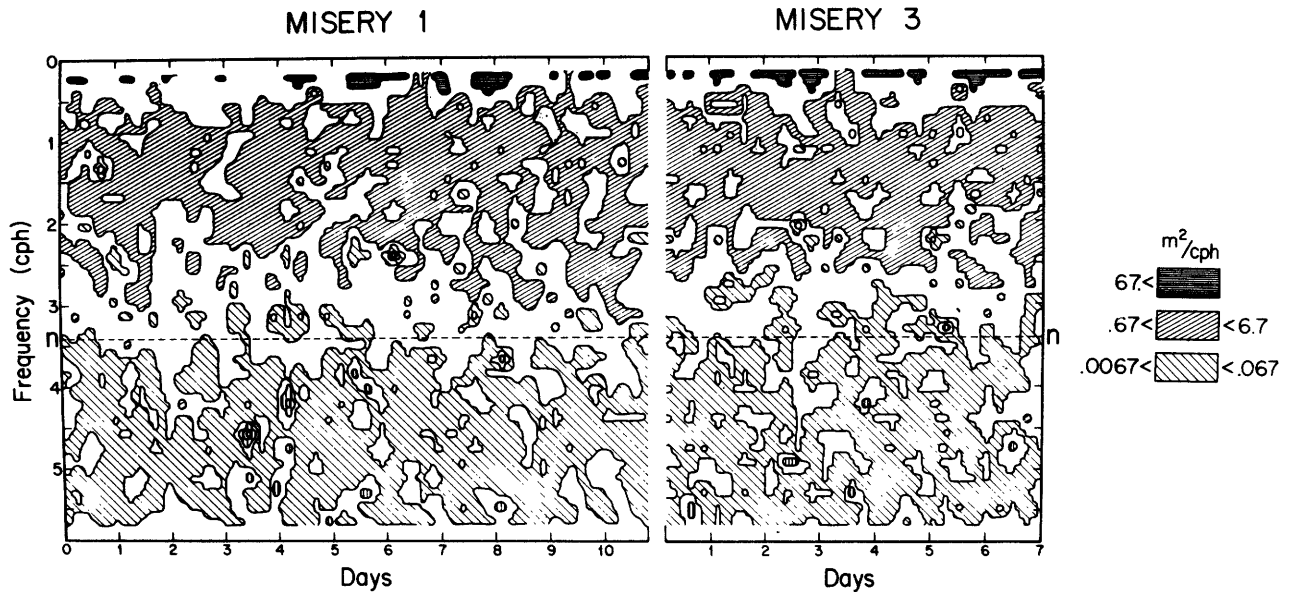


Figure 10.36 Contours of vertical-displacement spectral energy vs. elapsed time for the 6.60°C isotherm off the coast of southern California. Spatial estimates with 2 df are made for

successive 5.8-h data segments and the results are contoured. (Cairns and Williams, 1976.)

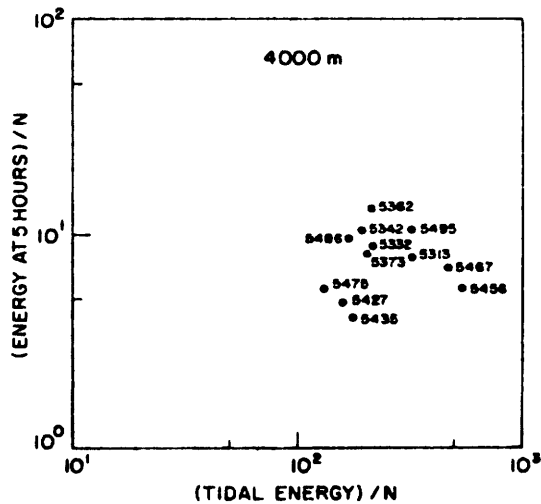


Figure 10.37 Five-hour internal wave energy at various locations vs. semidiurnal tidal energy. (Wunsch, 1976.)

ocean-current theory and through the work by Stommel and Arons (1960a,b) on abyssal circulation. Goldsbrough (1933) studied nonperiodic solutions of LTE driven by global patterns of evaporation and precipitation. The solutions are steady, provided that the precipitation–evaporation distribution vanishes when integrated along each parallel of latitude between basin boundaries. Stommel (1957b) pointed out that Ekman suction and blowing due to wind-stress convergence and divergence could effectively replace the evaporation–precipitation distribution, while the introduction of ageostrophic western boundary currents allowed the solutions to remain steady even when the integral constraint on the evaporation–distribution function was violated. The resulting flows display the main dynamic features of the theory of wind-driven circulation due to Sverdrup (1947), Stommel (1948), and Munk (1950). When the evaporation–precipitation function is viewed as modeling the high-latitude sinking of deep water and its mid-latitude subthermocline upwelling, the abyssal circulation theories of Stommel and Arons (1960a,b) result.

The seminal work on low-frequency second-class motions was the study (section 10.4.4) by Rossby and collaborators (1939), ironically inspired by meteorological rather than tidal studies. It led, through the studies by Veronis and Stommel (1956) and Lighthill (1969) of time-dependent motion generated by a fluctuating wind to the very different views of mid-latitudes and tropical transient circulation that prevail today (although, especially in mid-latitudes, linear dynamics

are now generally acknowledged to be inadequate for a full description; see chapter 5). Pedlosky (1965b) showed how the steady western boundary currents of Stommel (1948), Munk (1950), and Fofonoff (1954) could be viewed as Rossby waves reflected from the western boundary and either damped by friction or swept back toward the boundary by the interior flow that feeds the boundary current; Gates's (1968) numerical examples showed clearly the development of a frictional western boundary current as a group of short Rossby waves with seaward edge propagating away from the western boundary at the appropriate group velocity.

Modern interest in estimating the role of direct transient wind forcing in generating mesoscale oceanic variability (see chapter 11) calls for an up-to-date version of N. A. Phillips's (1966b) study of mid-latitude wind-generated Rossby waves using more realistic wind fields and taking into account new insight into the combined effects of bottom relief and stratification (section 10.4.7). Such a calculation would closely resemble a proper (linear) dynamic theory of long-period tides. But similar caveats apply to uncritically accepting either as representing an actual flow in the ocean.